The North America mid-Cretaceous kimberlite corridor: Wet, edge-driven decompression melting of an OIB-type deep mantle source

B. A. Kjarsgaard[1] , L. M. Heaman[2], C. Sarkar[2], and D. G. Pearson[2]

[1]Geological Survey of Canada, Ottawa, Ontario, Canada, [2]Department of Earth and Atmospheric Sciences, University of Alberta, Edmonton, Alberta, Canada

Abstract Thirty new high-precision U-Pb perovskite and zircon ages from kimberlites in central North America delineate a corridor of mid-Cretaceous (115–92 Ma) magmatism that extends ~4000 km from Somerset Island in Arctic Canada through central Saskatchewan to Kansas, USA. The least contaminated whole rock Sr, Nd, and Hf isotopic data, coupled with Sr isotopic data from groundmass perovskite indicates an exceptionally limited range in Sr-Nd-Hf isotopic compositions, clustering at the low ε_{Nd} end of the OIB array. These isotopic compositions are distinct from other studied North American kimberlites and point to a sublithospheric source region. This mid-Cretaceous kimberlite magmatism cannot be related to mantle plumes associated with the African or Pacific large low-shear wave velocity province (LLSVP). All three kimberlite fields are adjacent to strongly attenuated lithosphere at the edge of the North American craton. This facilitated edge-driven convection, a top-down driven processes that caused decompression melting of the transition zone or overlying asthenosphere. The inversion of ringwoodite and/or wadsleyite and release of H_2O, with subsequent metasomatism and synchronous wet partial melting generates a hot CO_2 and H_2O-rich protokimberlite melt. Emplacement in the crust is controlled by local lithospheric factors; all three kimberlite fields have mid-Cretaceous age, reactivated major deep-seated structures that facilitated kimberlite melt transit through the lithosphere.

Plain Language Summary A model is proposed in which molten rocks that are known to carry diamonds (kimberlites), are generated at great depth (>400 km) in the Earth, with the magma generation being facilitated by convection cells at the edge of the old North American craton

1. Introduction

Archetypal (Group I) kimberlite is formed from a volatile-rich (CO_2 and H_2O) ultrabasic magma that has an enriched incompatible (Ba, Nb, Zr, Hf, Ta, REE) and compatible (Ni, Cr, Co) trace element signature. These magmas give rise to a wide variety of landforms and intrusions similar to those associated with small-volume alkali basalt volcanic systems [*Kjarsgaard*, 2007]. Their scientific importance as a carrier of mantle xenoliths and diamonds and their inclusions has led to a significantly enhanced understanding of the Earth. However, despite decades of study the origin of the transport magma, kimberlite, remains controversial. It has been variably related to subduction processes [e.g., *Sharp*, 1974; *McCandless*, 1999; *Currie and Beaumont*, 2011], mantle plume hot spot tracks [e.g., *Crough et al.*, 1980; *le Roex*, 1986; *Heaman and Kjarsgaard*, 2000], mantle plumes associated with large superswell features in the mantle [e.g., *Torsvik et al.*, 2010, 2016], and precursory activity to major flood basalt events [e.g., *Heaman et al.*, 2003].

Additional issues are whether a precursor protokimberlite magma initially forms that subsequently reacts or evolves en-route to the surface to generate kimberlite magma, or if kimberlites are directly generated via low degrees of mantle partial melting. For example, protokimberlite magma has been previously suggested to be sourced from mantle plumes originating at the core—mantle boundary [*Haggerty*, 1994; *Torsvik et al.*, 2010], or from a transition zone source [*Ringwood et al.*, 1992; *Tappe et al.*, 2013]. Alternate models suggest primary kimberlite magma is generated from mantle plume metasomatized domains within the subcontinental lithospheric mantle (SCLM), e.g., *le Roex et al.* [2003]. Tracer isotopic studies (Sr-Nd-Hf) provide further insights into the nature of kimberlite source regions. Suggested source regions include the asthenosphere [*Smith*, 1983; *Zurevinski et al.*, 2011], the SCLM [*Tainton and MacKenzie*, 1994], mixing

between asthenosphere and SCLM [*Griffin et al.*, 2000], and in the transition zone or below [*Janney et al.*, 2002; *Nowell et al.*, 2004; *Paton et al.*, 2009; *Tappe et al.*, 2013; *Pearson et al.*, 2014].

In this study, we present new U-Pb isotope dilution thermal ionization mass spectrometry (ID-TIMS) analyses of groundmass perovskite and mantle zircon from archetypal kimberlites in the Somerset Island field in Nunavut, northern Canada, from the Fort à la Corne field and from the Sturgeon Lake kimberlite in central Saskatchewan. In addition, we present new TIMS perovskite strontium isotope, and whole rock strontium, neodymium, and hafnium isotope data from both fields. These new results are compared with published geochronology and Sr-Nd isotopic data for kimberlites from both fields and from Kansas, USA, which together define the central North America mid-Cretaceous kimberlite corridor. We synthesize all kimberlite data from this corridor to evaluate the mantle source region and geodynamic implications for the initiation and ascent of kimberlite magmatism, on a continental scale.

2. Background

2.1. Spatial-Temporal Distribution of Central North America Kimberlite Fields

The distribution of known kimberlites (fields, clusters, isolated occurrences) in North America is illustrated in Figure 1. *Heaman and Kjarsgaard* [2000] and *Zurevinski et al.* [2011] described the geochronology of Mesozoic (Triassic-Jurassic-Cretaceous) kimberlites in eastern North America, and their relationship to the Great Meteor hotspot track. *Heaman et al.* [2003, 2004] examined the ages of North American kimberlites within a global context, and described their temporal evolution and relation to tectonics in greater detail. These studies revealed the presence of a north-south trending central North American mid-Cretaceous (∼105–95 Ma) kimberlite corridor, with an extent of >4000 km (Figure 1). At the north end of the corridor is the Somerset Island kimberlite field, in the middle the central Saskatchewan kimberlite field (Fort à la Corne, Sturgeon Lake, Candle Lake), and at the south end the Riley and Marshall County kimberlites in northeast Kansas. Further to the south and along the same trend are the mid-Cretaceous Prairie Creek, Arkansas lamproites (Figure 1). Late Cretaceous kimberlites, ∼88 to 65 Ma in age are observed in the Buffalo Head Hills/Birch Mountains, Alberta [*Eccles et al.*, 2008], Wager Bay area, Nunavut [*Pell et al.*, 2008], Elliot County, Kentucky [*Heaman*, 1989], and Lac de Gras [*Heaman et al.*, 2003], as illustrated in Figure 1. These late Cretaceous kimberlites (excepting Elliot County) lie within the North American Craton and are distal to the attenuated craton edge; thus the magmatic processes for these localities is suggested to be distinct from those of the mid-Cretaceous corridor.

2.2. Previous Age Determinations of Kimberlites in Central North America

Previously published radiometric ages for kimberlites in central North America vary widely in age, ranging from Precambrian (Chicken Park, State Line field, Colorado; 614.5 Ma) to Tertiary (Williams, Missouri Breaks, Montana; 47.5 Ma), as summarized by *Heaman et al.* [2004]. Within the mid-Cretaceous corridor, Early to Late Cretaceous ages (∼113–88 Ma) have been previously published. *Smith et al.* [1989] reported three Somerset Island kimberlite ages: a Rb-Sr phlogopite age of ∼100 Ma for Batty K10 (Tunraq); a U-Pb ID-TIMS (perovskite) age of ∼105 Ma for the Georgia ultramafic lamprophyre (UML); and an age for the Elwin Bay kimberlite of ∼40 Ma that was considered unreliable. *Wu et al.* [2010] determined U-Pb perovskite ages of 113–96 Ma for kimberlites from Somerset Island utilizing laser ablation inductively coupled plasma mass spectrometry (LA-ICPMS) and secondary ion mass spectrometry (SIMS) methods.

In central Saskatchewan, previously reported kimberlite emplacement age dates range from 106 to 94 Ma. *Hegner et al.* [1995] determined a phlogopite Rb-Sr isochron age of 98 Ma for the Sturgeon Lake SL1 kimberlite. *Lehnert-Thiel et al.* [1992] reported Rb-Sr phlogopite model ages of ∼96 to 94 Ma from the Fort à la Corne field, and the #169 kimberlite body was determined to be 101 Ma by U-Pb ID-TIMS perovskite [*Leckie et al.*, 1997]. Subsequent studies on the Star and Orion South kimberlites in the Fort à la Corne field investigated in detail the multiple, discrete, and punctuated eruptive phases of these bodies, substantiated by ID-TIMS U-Pb perovskite ages of 104 and 103 Ma for Star [*Zonneveld et al.*, 2004], and 106, 104, and 99 Ma for Orion South [*Kjarsgaard et al.*, 2009a].

Studies on Kansas kimberlites by *Alibert and Albarède* [1988] and *Blackburn et al.* [2008] have yielded emplacement ages on four separate kimberlites between 106 and 103 Ma, and a fifth kimberlite possibly as
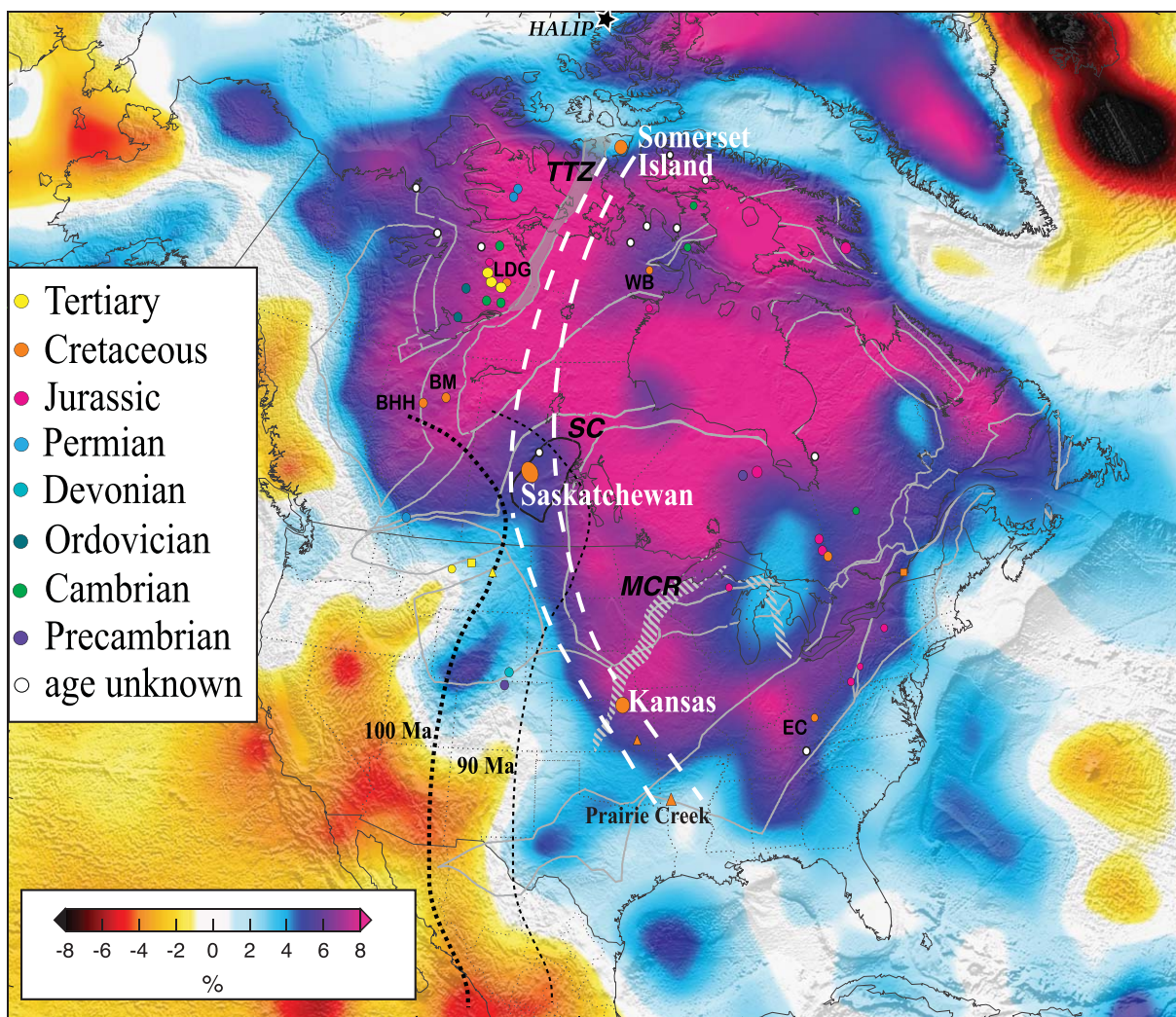
Figure 1. Location map of kimberlite pipes, clusters and fields in North America, with the mid-Cretaceous kimberlite corridor demarcated by white-dashed lines. The eastern (leading) edge of Farallon slab in central North America at 100 and 90 Ma (at 403 km depth) are shown as thick and thin black-dashed line, respectively [after *Spasojevic et al.*, 2009]. Map symbols: circles, kimberlites; triangles, lamproites; and squares, ultramafic lamprophyres. All symbols are color coded by age (see legend), with white symbols indicating age unknown. Kimberlite locations and ages modified after *Heaman et al.* [2003, 2004]. MCR = Midcontinent Rift (grey hachure); SC = Sask Craton (outlined by black solid line); TTZ = Thelon Tectonic Zone (grey fill); HALIP = location of proposed HALIP plume head, present-day [from *Buchan and Ernst*, 2006] WB = Wager Bay kimberlites; LDG = Lac de Gras kimberlites; BHH = Buffalo Head Hills kimberlites; BM = Birch Mountains kimberlites; EC = Elliot County kimberlite. Figure backdrop is the mantle shear-speed structure at 150 km depth (SL2013NA) and major tectonic boundaries (light grey lines), from *Schaeffer and Lebedev* [2014].

young as 88 Ma. The study by *Blackburn et al.* [2008] utilized the (U + Th)/He age dating methodology on a variety of minerals, as well as age determinations by Rb-Sr on phlogopite.

2.3. Application of Perovskite for U-Pb Geochronology and Tracer Isotopic Studies

U-Pb dating of groundmass perovskite was initially investigated using the ID-TIMS method on perovskite-rich concentrate[(*Kramers and Smith*, 1983; *Smith et al.*, 1989], pure perovskite fractions [*Heaman*, 1989], and more recently by spatially resolved in situ methods (ion microprobe: *Kinny et al.* [1997]; *Wu et al.* [2010]; *Sun et al.* [2014]) or LA-ICPMS techniques [*Cox and Wilton*, 2006; *Wu et al.*, 2010, 2013]. Perovskite ($CaTiO_3$) is a groundmass mineral that is observed in ultramafic and mafic, silica-undersaturated, subalkaline, and alkaline rocks e.g., kimberlite, carbonatite, nephelinite, melilitite, and ultramafic lamprophyre (UML). The abundance of perovskite in kimberlite is quite variable (trace to 15%) [*Mitchell*, 1995], and although often considered a common groundmass phase, it may be rare or even absent [*Clement et al.*, 1984; *Sarkar et al.*, 2015]. The timing of perovskite crystallization in kimberlite magma is variable, typically after olivine and Cr, Mg-spinel and prior to monticellite, calcite, and groundmass phlogopite [*Mitchell*, 1986]. However, it can also have a more protracted crystallization

history (intermediate to late) [*Malarkey et al.*, 2010], or only as a late phase cocrystallizing with Fe-Ti spinel and magnetite [*Sarkar et al.*, 2013].

In kimberlite, perovskite grain size is quite variable, ranging from <5 to >100 μm, although 20–60 μm grains seem to predominate. *Heaman* [1989] and *Smith et al.* [1989] originally suggested that perovskite should record the primary geochemical and isotopic signature with respect to the timing of emplacement and origin of the kimberlitic magma, prior to any contamination and weathering, based on TIMS U-Pb and Sr-Nd isotopic studies on perovskite. More recent isotopic studies on perovskite by *Paton et al.* [2007], *Wu et al.* [2010, 2013], *Zurevinski et al.* [2011], *Sarkar et al.* [2014, 2015], and *Sun et al.* [2014] have further established these concepts. However, the Sr isotopic study of *Malarkey et al.* [2010] demonstrates perovskite recording crustal contamination, suggesting some caution needs to be exercised.

2.4. Kimberlite Sample Suites
The Somerset Island kimberlite field [*Mitchell*, 1975] is hosted by Cambro-Ordovician to Silurian dolomite and limestone. These rocks are underlain by Proterozoic sedimentary rocks, and older gneiss and granitoid rocks [*Kjarsgaard*, 1996a, 1996b] that are on the northern periphery of the Rae Craton [*Aspler and Chiarenzelli*, 1998], adjacent to the Thelon Tectonic Zone (Figure 1). The kimberlite samples investigated were collected from outcrop, subcrop, or large frost-heaved boulders, and consist of hypabyssal (coherent) kimberlite. Sample size typically ranged from 0.2 to 2 kg. Additional details of the samples, locations, and geochronology are provided in supporting information S1.

Kimberlites in central Saskatchewan occur on the eastern margin of the Western Canadian Sedimentary Basin [*Lehnert-Thiel et al.*, 1992; *Leckie et al.*, 1997]. Platformal sediments overlie Paleoproterozoic basement rocks (Glennie Domain of the Trans-Hudson Orogen), which in turn overlie the Archean Sask Craton [*Lucas et al.*, 1993] (Figure 1). The host rocks consist of Cretaceous siliciclastic sandstone, siltstone, and shale of the Manville Group (Cantuar and Pense formations), which are overlain by marine sediments (dominantly shale) of the Colorado Group (Joli Fou, Viking, Westgate, and Belle Fourche formations). The sample suite is comprised of primary volcaniclastic kimberlite, and two hypabyssal (coherent) samples. The kimberlite volcanic rocks are assigned to the sedimentary strata in which they are intercalated, e.g., Cantuar-equivalent kimberlite, when this is known. The kimberlite samples investigated in this study were collected from drillcore, excepting the Sturgeon Lake samples that are from an ice-rafted megalith "outcrop." Additional details of the samples, locations, and geochronology are provided in supporting information S1.

3. Analytical Methods

The methods for the whole rock Sr-Nd-Hf isotope analyses, Sr isotope analyses on perovskite, and U-Pb geochronology on perovskite and zircon are described in detail in supporting information S2.

4. Results

4.1. Somerset Island Kimberlite Field U-Pb ID-TIMS Perovskite Ages
The seven new U-Pb perovskite ages indicate three periods of magmatism on Somerset Island (Table 1, Figure 2, supporting information Table S1): previously unknown Carboniferous UML magmatism at 300 Ma, and two distinct periods of Cretaceous kimberlite magmatism at 97 Ma (Elwin-Jos-Batty-Ham) and 93 Ma (Peuyuk). The apparent dichotomy between the 300.5 Ma age of the Cresswell UML (this study) and the 105 Ma age for the nearby Georgia UML [*Smith et al.*, 1989] is explained by a potential switch of the Elwin Bay and Georgia samples (C. B. Smith, written communication, 1994) i.e., Elwin Bay kimberlite is ~105 Ma, in general agreement with our new U-Pb perovskite age for this locality, with the 40 Ma age for the Georgia UML being unreliable [*Smith et al.*, 1989].

4.2. Central Saskatchewan Kimberlite Field U-Pb ID-TIMS Perovskite and Zircon Ages
The 23 new U-Pb perovskite and mantle zircon ages from 12 separate kimberlite bodies indicate that magmatism in the central Saskatchewan kimberlite field spanned the time interval from 115 to 92 Ma. These new ages, along with previous age determinations (section 2.2.) indicate the peak of magmatic activity (23 of 25 dated kimberlites) occurred over 8 million years, between 103.2 and 95.5 Ma (Table 1, Figure 3, supporting information Table S1). A precursor event at ~115 Ma, and a late event at 92.5 Ma extend the period

Table 1. Radiometric Age Determinations for mid-Cretaceous North American Kimberlites

Locality	Age	± (2σ)	Method	# of Fractions
Somerset Island kimberlite field, Nunavut, Canada				
Cresswell	300.5	1.2	Perovskite	1
Batty K10 (Tunraq)	97.1	1.1	Perovskite	3
Batty K12	97.3	1.8	Perovskite	2
Elwin Bay	96.4	1.8	Perovskite	2
Ham dyke	96.8	2.1	Perovskite	2
Jos dyke	97.5	1.4	Perovskite	2
Peuyuk phase C	92.8	2.5	Perovskite	2
Central Saskatchewan kimberlite field, Saskatchewan, Canada				
Star 13 (Cantuar)	102.1	1.4	Perovskite	2
Star 20 (EJF)	102.7	2.0	Perovskite	1
Star 6 (EJF)	101.0	1.5	Perovskite	2
Star 20 (MJF)	102.1	1.6	Perovskite	1
Star 30 (late sill)	99.5	1.2	Perovskite	2
Orion South (Cantuar)	103.2	2.4	Perovskite	1
Orion South (P2)	103.3	2.0	Perovskite	2
Orion South (P3)	101.0	3.8	Perovskite	1
Orion South (EJF-2)	99.3	0.3	Perovskite	4
Orion South (BF)	95.5	2.6	Perovskite	1
FalC #101	100.2	2.0	Perovskite	2
FalC #118	95.7	1.2	Perovskite	2
FalC #120	98.5	1.2	Perovskite	1
FalC #121	96.7	3.8	Perovskite	2
FalC #145 (EJF)	99.5	1.7	Perovskite	2
FalC #145 (EJF)	101.0	2.4	Perovskite	1
FalC #169 (EJF)	100.8	2.2	Perovskite	1
FalC #181	98.2	2.8	Perovskite	1
FalC #226	99.9	1.8	Perovskite	3
FalC-5	114.7	8.4	Perovskite	1
Sturgeon Lake	98.8	0.2	Zircon	1
Sturgeon Lake BK1	95.5	0.2	Zircon	1
Sturgeon Lake BK5	92.5	0.2	Zircon	1

of magmatism to ∼23 million years. For kimberlite volcanic samples with radiometric age determinations that are bracketed by Cretaceous sediments assigned to a specific sedimentary formation, the U-Pb and bio-stratigraphic ages are consistent (supporting information S1). The majority of the larger kimberlite bodies in this field are not the result of a single monogenetic emplacement episode. Rather, they are best described as composites of stacked, monogenetic volcanoes that formed in distinct pulses over one to several million years [*Kjarsgaard*, 2007].

4.3. Tracer Isotopic Results

New whole rock Sr, Nd, and Hf tracer isotopic data for Somerset Island and central Saskatchewan kimberlite samples are listed in supporting information Table S2, along with perovskite Sr isotopic data from a subset of samples. Comparative tracer isotopic studies on kimberlite whole rocks and perovskite separates have shown that crustal contamination and postemplacement alteration can modify the Sr isotopic composition of the whole rock, with the perovskite retaining a "primary" signature [e.g., *Heaman*, 1989; *Paton et al.*, 2007]; the Sr isotope results obtained in this study confirm this assertion. For Somerset Island kimberlites, TIMS Sr isotopic data for perovskite define a limited range of $^{87}Sr/^{86}Sr(i)$ of 0.704680–0.705013. Our new data are compared with whole rock TIMS data, microdrilled perovskite TIMS data [*Malarkey et al.*, 2010], and perovskite LA-MC-ICPMS data [*Wu et al.*, 2013] in Figure 4a.

A direct comparison of whole rock and perovskite data (Peuyuk, Elwin Bay, Ham dyke, Jos dyke, Batty K10-Tunraq samples) indicates that the perovskite $^{87}Sr/^{86}Sr(i)$ measurements are consistently lower than the whole rock. Batty Bay K10 kimberlite samples have a significant spread in perovskite $^{87}Sr/^{86}Sr(i)$, possibly suggesting crustal contamination (Figure 4a). For other Batty Bay complex samples, there is overlap between the whole rock Sr isotopic data and the perovskite LA-MC-ICPMS data, but the analyses cannot be directly compared because the specific locations of the kimberlites studied by *Wu et al.* [2013] were not identified. For Somerset Island kimberlites, the least radiogenic perovskite Sr isotopic data is $^{87}Sr/^{86}Sr(i) = 0.7046$ to 0.7051, based on TIMS or LA-MC-ICPMS data (Figure 4a). For central Saskatchewan kimberlites, perovskite separates from six samples have a more restricted range and lower $^{87}Sr/^{86}Sr(i)$ of
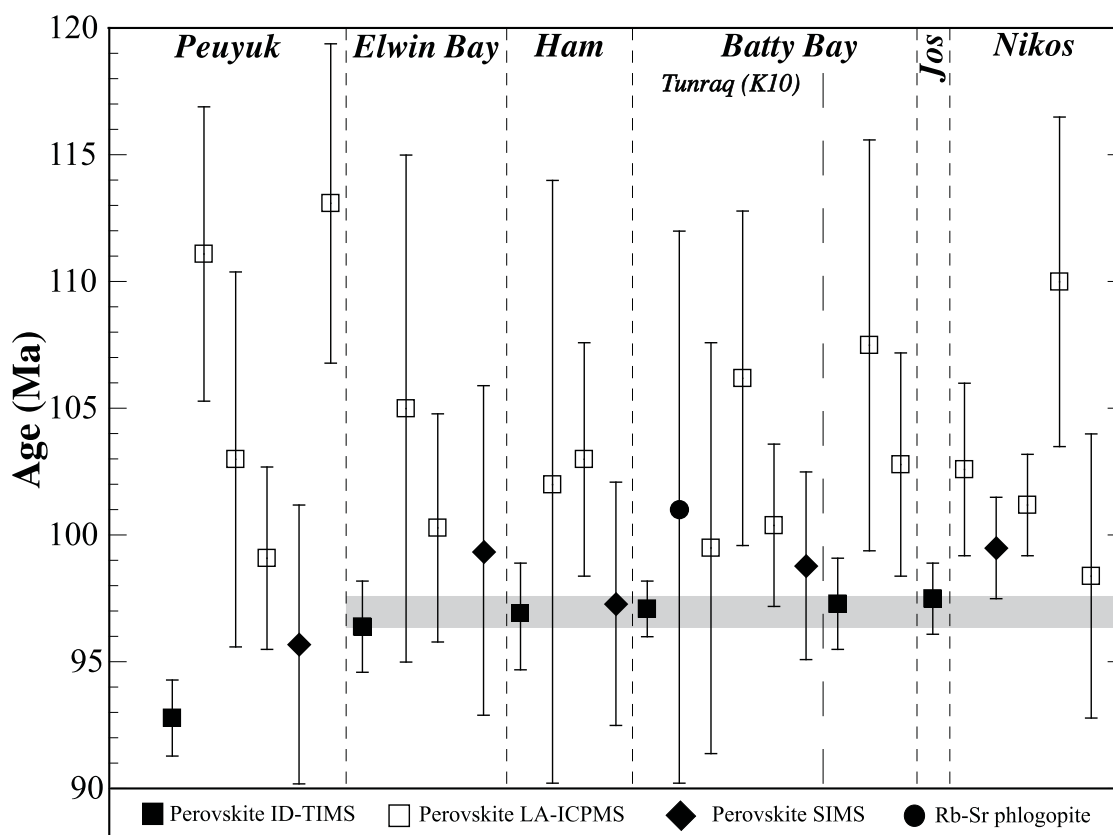
Figure 2. New U-Pb perovskite ages (with 2σ uncertainty) for Somerset Island kimberlites determined by ID-TIMS (this study), compared to perovskite ages determined by LA-ICPMS and SIMS [*Wu et al.*, 2010]. Vertical-dashed lines separate kimberlite localities. The Rb-Sr phlogopite age for Batty K10 (Tunraq) determined by *Smith et al.* [1989] is also shown. The grey horizontal band encompasses the perovskite data from this study, for five separate kimberlite intrusions of similar age. The long-dashed vertical line separates age determinations for the Batty K10 (Tunraq) kimberlite from other individual kimberlite bodies within the Batty Bay complex.

0.70479–0.70507 as compared to six whole rock samples, with $^{87}Sr/^{86}Sr(i)$ of 0.70541–0.70699 (Figure 4b). For central Saskatchewan kimberlites, the least radiogenic perovskite Sr isotopic data is $^{87}Sr/^{86}Sr(i)$ = 0.7048–0.7051, based on TIMS perovskite data (Figure 4b).

Whole rock Sr and Nd isotopic data are plotted in Figure 5a, and shown with previously published data for Somerset Island [*Schmidberger et al.*, 2001], Saskatchewan [*Hegner et al.*, 1995], and from Kansas [*Alibert and Albarède*, 1988]. In addition, we have plotted three Somerset Island samples on Figure 5a utilizing the perovskite TIMS Sr data with the whole rock Nd isotopic data (perovskite and whole rock derived from the same sample), following the tactic of *Paton et al.* [2009]. Nd and Sr tracer isotope data on perovskite [*Wu et al.*, 2010, 2013] from Somerset Island are also plotted for comparison (Figure 5a). We define the primary Somerset Island kimberlite Sr-Nd isotopic composition as $^{87}Sr/^{86}Sr(i)$ = 0.7046–0.7051 (perovskite; Figures 4a and 5b) and εNd(i) = −0.17 to +1.95 (whole rock, perovskite) as illustrated in Figure 5b. For the Saskatchewan kimberlites, the combined Sr-Nd isotopic composition is defined by the $^{87}Sr/^{86}Sr(i)$ values of 0.7048–0.7051 in perovskite (Figure 4b and 5b), coupled with the whole rock εNd(i) data of +0.15 to +1.30 (Figure 5b). For Kansas kimberlites there is a paucity of data, however, we use the whole rock εNd isotope data of *Alibert and Albarède* [1988] (εNd (i) = +1.1 to +1.5) combined with the strontium isotopic composition of 0.704485 (Figure 5b), derived from the $^{87}Sr/^{86}Sr(i)$ value projected from the Rb-Sr phlogopite isochron of *Blackburn et al.* [2008]. The whole rock $^{87}Sr/^{86}Sr(i)$ values of 0.70615–0.70688 (data of *Alibert and Albarède*, [1988]) for the Kansas kimberlites are not utilized as these radiogenic values are likely too high, consistent with the studied samples being country-rock contaminated breccias.

For a subset of Somerset Island and Saskatchewan kimberlite samples, Lu-Hf whole rock isotopic compositions were also determined. These data are plotted on a εHf(i) versus εNd(i) diagram (Figure 5c), and form a compact cluster with εHf(i) ranging from 0 to +3.9 and εNd(i) from +0.15 to +1.95, straddling the mantle
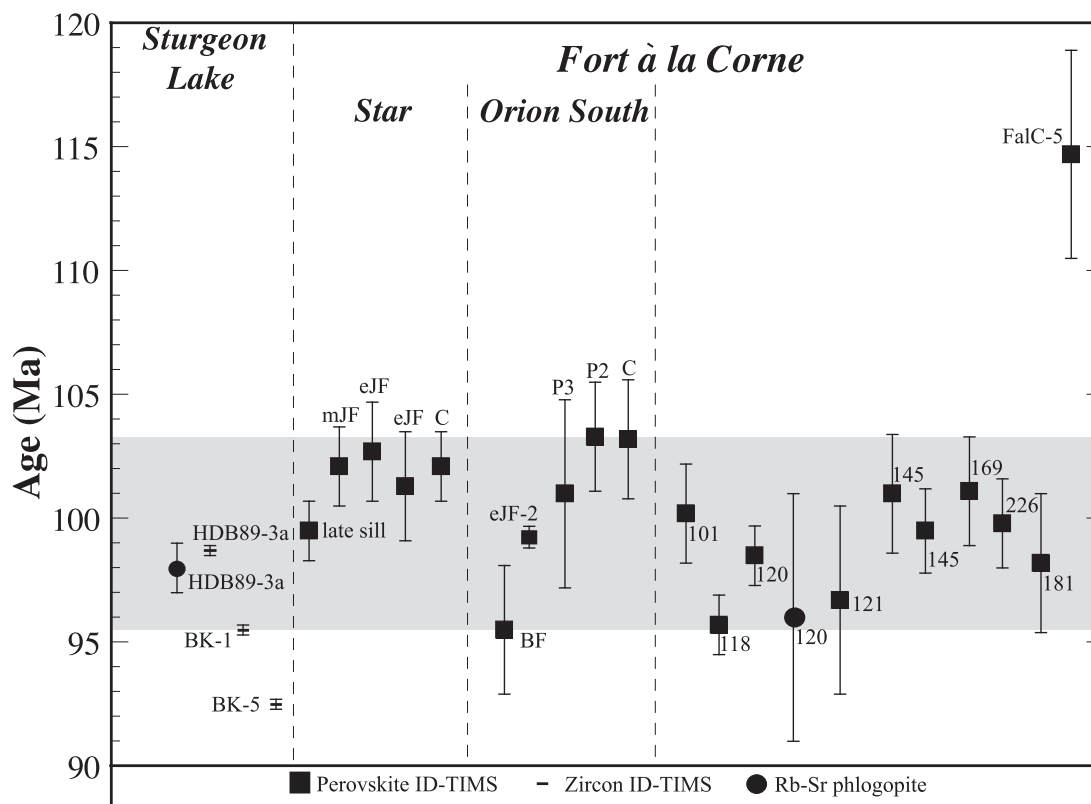
Figure 3. New U-Pb ID-TIMS perovskite and zircon age determinations (this study), and phlogopite Rb-Sr ages (all with 2σ uncertainty) for samples from the central Saskatchewan kimberlite field. The grey band encompasses the main period of kimberlite volcanism in central Saskatchewan (103–95 Ma). The Star, Orion South and Sturgeon Lake kimberlites have multiple discrete magmatic events with individual age determinations. For Star and Orion South, labels indicate the equivalent stratigraphic formation of the volcanic rocks: C = Cantuar; P = Pense; eJF = early Joli Fou; mjF = mid Joli Fou; BF = Belle Fourche Fm (see also supporting information Figure S1). For kimberlite bodies with only one age determination, or poorly resolved stratigraphic constraints on volcanism, only the kimberlite body I.D.# is shown. Two Rb-Sr phlogopite isochron ages, from *Hegner et al.* [1995] for Sturgeon Lake, and from Lehnert-*Thiel et al.* [1992] and *Scott-Smith* [2008] for the #120 kimberlite are also shown.

Nd-Hf isotope regression line of *Chauvel et al.* [2008]. The Somerset and Saskatchewan kimberlites plot in an intermediate area in εHf(i) versus εNd(i) isotopic space between the Jurassic Jericho [*Dowall*, 2004] and Late Cretaceous to Eocene Lac de Gras [*Dowall*, 2004; *Tappe et al.*, 2013] kimberlites (Figure 5c).

The utilization of whole rock tracer isotopic data for Nd and Hf, coupled with TIMS Sr isotopic data from perovskite separates is considered here to provide a robust primary tracer isotopic signature of the mantle sources of mid-Cretaceous kimberlites from Somerset Island and central Saskatchewan. We further note that in Sr-Nd-Hf isotopic space, the Somerset and Saskatchewan data sets are extremely similar. Kansas kimberlites have similar Sr-Nd to kimberlites from Somerset and Saskatchewan, but this assertion requires testing with additional data. All North American mid-Cretaceous corridor kimberlites lie within, and at the low ε_{Nd} end of the OIB array as defined by *Hofmann* [2014], and are isotopically distinct compared to other North American kimberlites (Figure 5b).

5. Discussion

5.1. Geochronology of Mid-Cretaceous Kimberlites in Central North America
New U-Pb perovskite ID-TIMS age data for six kimberlites from the Somerset Island field (Elwin Bay, two intrusions at Batty Bay, Peuyuk, Ham dyke and Jos dyke) highlight the very narrow time span (97.5–92.8 Ma) for emplacement of these kimberlites (Figures 2 and 6). Apart from the older ultramafic lamprophyres (the 300 Ma Cresswell intrusion), and the slightly younger Peuyuk kimberlite (92.8 Ma), all other kimberlites were emplaced between 97.5 and 96.4 Ma (Figure 2; horizontal grey bar). The Peuyuk ID-TIMS perovskite date of 92.8 Ma is considered significant and robust, as the upper bound on the Peuyuk age determination is younger than the lower bound on any age determination for the other kimberlites (Figure 2).
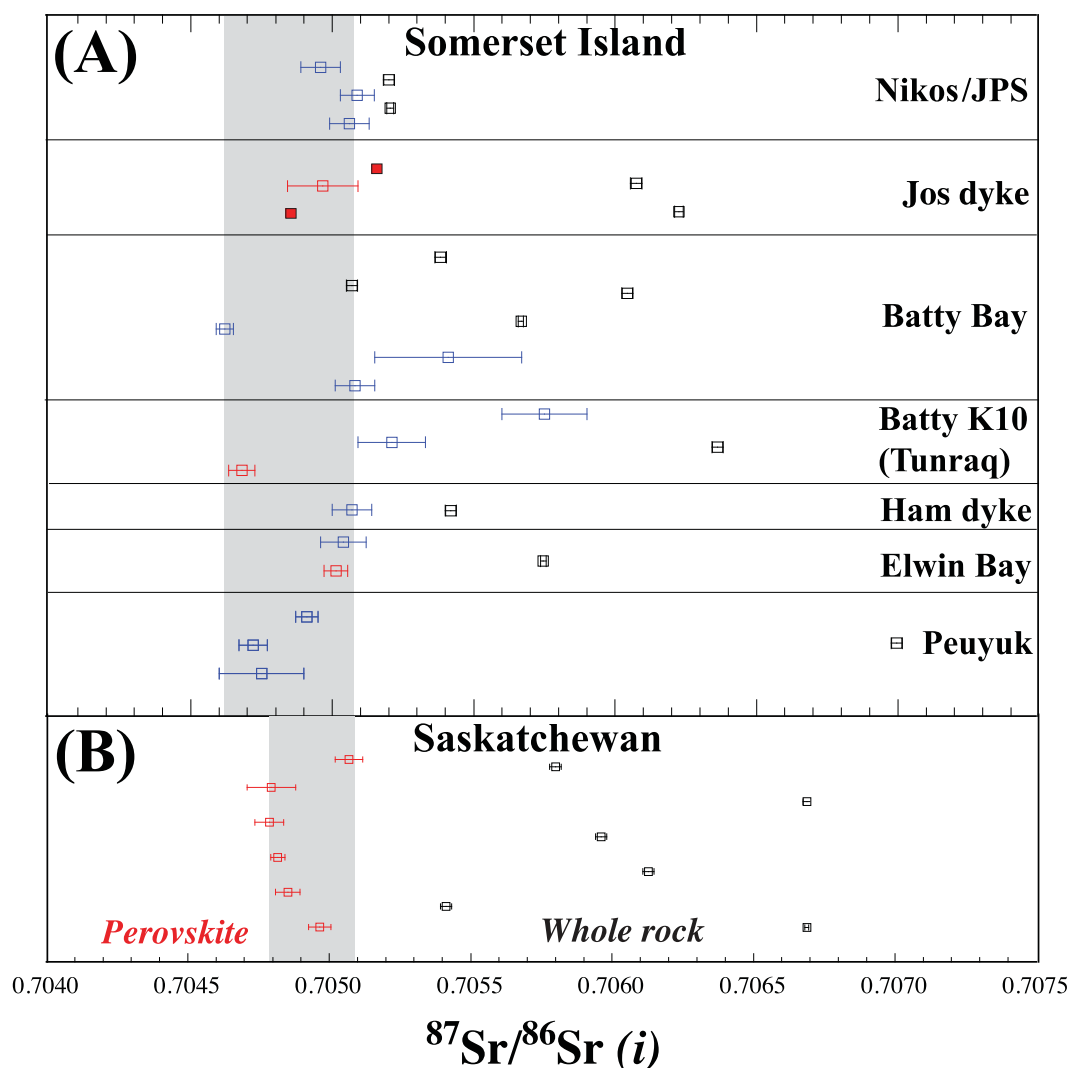
Figure 4. (a) Somerset Island kimberlites, comparison of TIMS ^{87}Sr/^{86}Sr(i) from perovskite (this study; red symbols), with the TIMS results from microdrilling of perovskite (filled red symbols) from the Jos dyke [*Malarkey et al.*, 2010], LA-MC-ICPMS on perovskite (blue symbols; *Wu et al.* [2013]), and whole rock data (black symbols: this study; and *Schmidberger et al.* [2001]). The grey band represents the range of least radiogenic ^{87}Sr/^{86}Sr(i) by TIMS or LA-MC-ICPMS on perovskite. (b) Saskatchewan kimberlites, comparison of TIMS ^{87}Sr/^{86}Sr(i) from perovskite (red symbols; this study) with whole rock data (black symbols: this study, and *Hegner et al.*, [1995]). The grey band represents the range of ^{87}Sr/^{86}Sr(i) by TIMS on perovskite.

Comparing perovskite U-Pb dating methods, the SIMS perovskite ages presented by *Wu et al.* [2010] are within error of our ID-TIMS perovskite ages for any given locality, but the SIMS ages are all systematically older (0.5–3.0 Ma) with appreciably larger age uncertainties (±3.7 to ±6.5 Ma) compared to the ID-TIMS data (±1.1 to ±2.1 Ma). The LA-ICPMS perovskite ages presented by *Wu et al.* [2010] are also within error of the ID-TIMS perovskite ages for any given locality (excepting Peuyuk; Figure 2), but are also always systematically older (2.4–20.3 Ma), with significantly larger uncertainties on the age (±3.2 to ±12.0 Ma). On the basis of the smaller uncertainties of the ID-TIMS data, we consider these to be the most robust in the compiled data set. The ID-TIMS results indicate that Somerset Island kimberlites were emplaced at 97.5–96.4 Ma (Jos-Elwin-Batty-Ham-Jos) and at 92.8 Ma (Peuyuk) i.e., the magmatism occurred over a ∼5 million year time span (Figure 6). The Nikos/JPS kimberlite is possibly as old as 100 Ma (Figures 2 and 6) based on the SIMS date reported by *Wu et al.* [2010], but further high-precision ID-TIMS U-Pb perovskite dating is required to confirm this.

In central Saskatchewan, our new U-Pb age results indicate that volcanism started with a precursor event at 115 Ma, followed by the volumetrically dominant period of kimberlite eruptions during the relatively short

interval between 103.2 and 95.5 Ma, i.e., an 8 million year time window (Figures 3 and 6). The Rb-Sr phlogo-pite result of *Hegner et al.* [1995] for Sturgeon Lake (98.0 ± 1.0 Ma) is in excellent agreement with our new U-Pb zircon age (98.8 ± 0.2 Ma), from a split from the same sample. Two other Rb-Sr phlogopite ages from Fort à la Corne are quoted in the literature [*Lehnert-Thiel et al.*, 1992; *Scott-Smith*, 2008], however, it is diffi-cult to assess how robust these ages are due to insufficient supporting analytical data. We caution against accepting the 94 ± 3 Ma Rb-Sr phlogopite age as a good estimate for the emplacement age of the #122 kimberlite body due to the reported high initial Sr isotopic composition, with $^{87}Sr/^{86}Sr(i) = 0.709$ (see *Sarkar et al.* [2015] for a detailed discussion of limitations with Rb-Sr kimberlite geochronology). The 96 Ma Rb-Sr phlogopite age for the #120 body [*Lehnert-Thiel et al.*, 1992] is considered reliable because the reported ini-tial strontium isotopic composition ($^{87}Sr/^{86}Sr(i) = 0.705$) is similar to and consistent with the new Fort à la Corne perovskite TIMS Sr isotopic results presented in this study.

The robust U-Pb ages from Somerset Island (Figure 2) and U-Pb and Rb-Sr ages for Saskatchewan (Figure 3) are compiled along with published data for Kansas kimberlites in Figure 6. Four Kansas kimberlites have age determinations in the range 109–103 Ma (Figure 6). A fifth, the Baldwin Creek kimberlite is reported to be younger (88 Ma), however, the phlogopite isochron initial Sr isotopic composition is extremely high ($^{87}Sr/^{86}Sr(i) = 0.75$), indicating significant crustal contamination and the age is likely unreliable. The (U + Th)/He age on apatite (86 Ma) for Baldwin Creek is similar, but contrasts with all other apatite ages (63.2–67.3 Ma, for three kimberlite samples) from the study of *Blackburn et al.* [2008] that were interpreted to be re-set at ∼65 Ma.

Considering only the more robust perovskite, zircon and phlogopite geochronology data indicate that mid-Cretaceous kimberlite magmatism in central North America occurred from 115 to 92 Ma (Figure 6). In detail however, the duration of the majority of magmatism in each kimberlite field is more limited (typically <10 million years), 97.3–92.8 Ma (4.5 Ma duration) at Somerset Island, 103.3–95.5 Ma (7.8 Ma duration) in central Saskatchewan, and 109–103 Ma (∼6 Ma duration) in Kansas. An interesting feature of the timing of kimber-lite emplacement along this corridor is that despite there being overlap in emplacement dates between the three main kimberlite fields, there appears to be an age progression in the main period of kimberlite activity from south to north, i.e.; 109–103 Ma for the Kansas kimberlites, 103–95 Ma in Central Saskatchewan, and 98–93 Ma at Somerset Island.

Mid-Cretaceous alkaline magmatism in North America also occurs in Arkansas, e.g., the 106 ± 3 Ma Prairie Creek lamproite [*Gogenini et al.*, 1978], the 105.7 ± 1.1 Ma Dare Mine Knob lamproite [*Eby and Vasconcelos*, 2009] and a range of dates between 104 and 94 Ma for the Magnet Cove alkaline complex and associated car-bonatite dykes [*Baksi*, 1999; *Eby and Vasconcelos*, 2009]. It is likely therefore that the mid-Cretaceous corridor defined here extends even further south. Although the timing of alkaline and lamproite magmatism in Arkan-sas is coeval with the magmatism occurring in the three mid-Cretaceous kimberlite fields, the magma compo-sitions are distinct and their radiogenic isotope compositions variable. For example, a 100 Ma carbonatite from the Magnet Cove complex has a strontium (0.70521) and neodymium (εNd +2.0) isotopic composition [*Duke et al.*, 2014] similar to some mid-Cretaceous kimberlites. However, the 106 Ma Prairie Creek lamproite has a radiogenic initial Sr (0.7069–0.7071) [*Alibert and Albarède*, 1988; *Heaman*, 1989], with neodymium isoto-pic composition for perovskite and whole rocks varying between εNd values of −10.1 to −13.0, consistent with derivation from the subcontinental lithospheric mantle [*Heaman*, 1989; *Duke et al.*, 2014].

The relatively short duration of kimberlite magmatism in the mid-Cretaceous corridor contrasts with the typi-cally longer periods of magmatism recorded by other kimberlite fields in western North America, e.g., Late Cretaceous (88–68 Ma) kimberlites from the Buffalo Head Hills, Alberta [*Eccles et al.*, 2008], or Late Cretaceous to Paleogene (75–45 Ma) kimberlites from the Lac de Gras area, Northwest Territories [*Heaman et al.*, 2004; *Sarkar et al.*, 2015]. Late Cretaceous kimberlites at Wager Bay, Nunavut [*Pell et al.*, 2008], and Elliot County, Ken-tucky [*Heaman*, 1989; *Heaman et al.*, 2004] are distal to the east of the mid-Cretaceous kimberlite corridor (Fig-ure 1) and are significantly younger (87–70 Ma).

5.2. Regional Tectonic and Structural Controls on the Location of the Kimberlites

The existence of a central corridor of mid-Cretaceous kimberlite magmatism in North America [*Heaman et al.*, 2003, 2004] provokes the question of why kimberlite magmatism is only observed in Kansas, Saskatch-ewan, and Somerset Island within the more extensive mid-Cretaceous corridor. Hence we examine the regional structure and tectonics of the lithosphere for each kimberlite field, which is very relevant to the
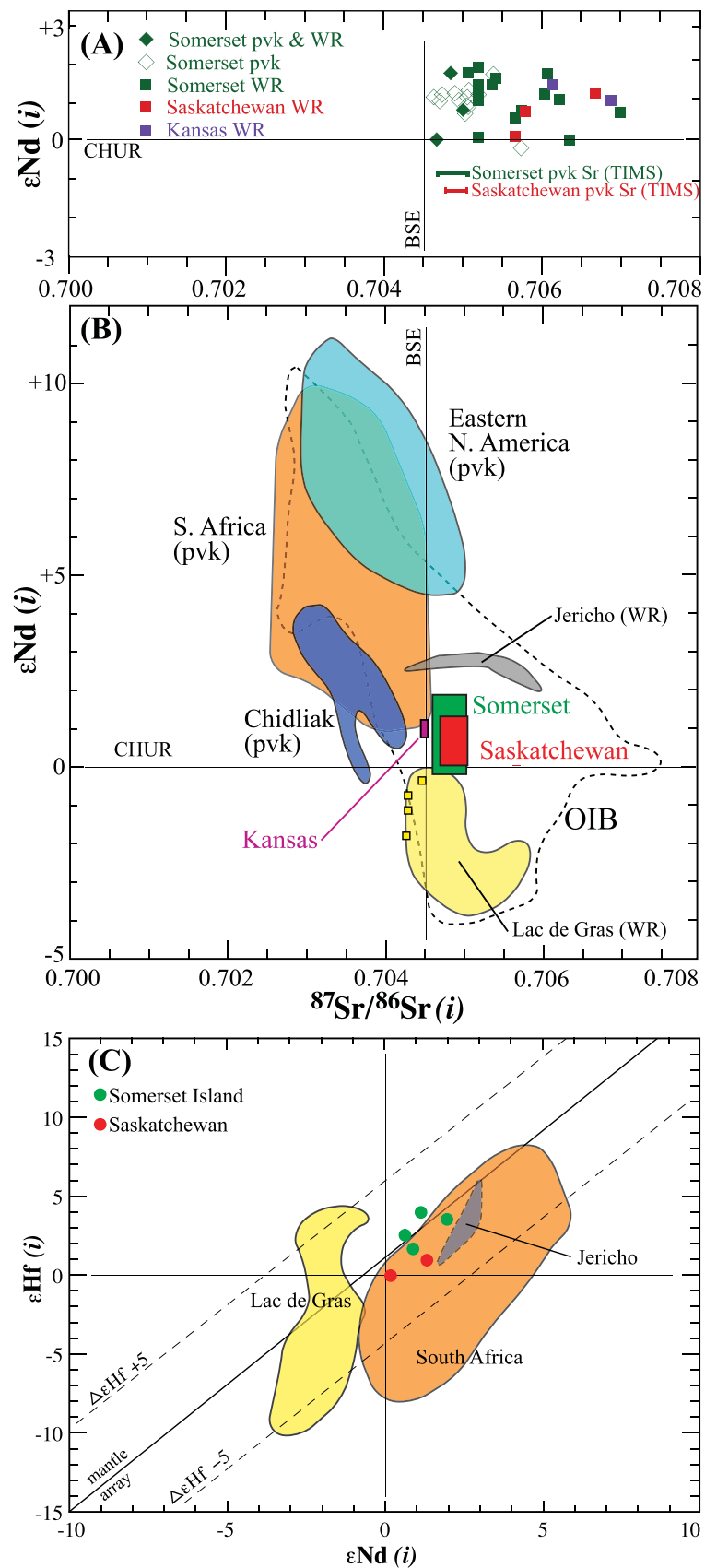
Figure 5. (continued)

problem of small volume magmas traversing the lithosphere. In this regard, previous studies recognized a strong structural control on kimberlite emplacement in the crust [e.g., *Nixon*, 1973; *Haggerty*, 1982; *White et al.*, 1995; *Jelsma et al.*, 2009]; they are typically located on splays off of major crustal breaks, or at the intersection of major crustal breaks.

5.2.1. Somerset Island Kimberlites

Somerset Island kimberlite magmatism occurs within a tectonic quiet period in the region, it is much younger than the Late Silurian-Early Devonian Boothia Uplift, and older than the Late Cretaceous to Oligocene Eurekan Orogeny [*Trettin*, 1991]. Tholeiitic magmatism is observed ∼250 km north of Somerset Island, at the southern edge of the High Arctic Large Igneous Province (HALIP) in the Sverdrup Basin. This magmatism was manifest as five or six pulses from ∼130 to 80 Ma [*Villenueve and Williamson*, 2006, and references therein]. Approximately coeval with kimberlite magmatism on Somerset Island are the Strand Fjord Formation volcanic rocks and associated intrusions, with age determinations of ∼97–96 Ma and ∼94–92 Ma [*Villenueve and Williamson*, 2006] i.e., overlapping the range of Somerset Island kimberlite emplacement ages.

Two significant basin margin unconformities occur in the stratigraphic record in the Sverdrup Basin, between the Hassel and Bastion Ridge formations, and the Bastion Ridge and Kanguk formations at ∼100 and ∼97 Ma, respectively [*Embry and Beauchamp*, 2009; *Herrle et al.*, 2015] and are coeval to slightly older than the age of the kimberlite magmatism. Based on stratigraphic evidence, the unconformities are interpreted as uplift related to the mafic magmatism [*Embry and Beauchamp*, 2009], and/or a change from rift to drift in the adjacent Amerasia Basin [*Embry and Dixon*, 2000]. We interpret that tectonomagmatic reactivation of preexisting NW-SE and Thelon Tectonic Zone-related N-S trending basement faults on Somerset Island (Figure 1 and supporting information S1) allowed for ascent of the small volume kimberlite magmas through the upper lithosphere at ∼97 to 93 Ma. Note however, this kimberlite emplacement age-tectonomagmatic relationship is revealed only when applying the high-precision ID-TIMS U-Pb perovskite age results of this study, but not if the LA-ICPMS or SIMS geochronology data of *Wu et al.* [2010] is utilized for the comparison, due to the scattering of ages (97–113 Ma) produced by those techniques.

5.2.2. Central Saskatchewan and Kansas Kimberlites

Based on detailed analysis of sedimentary deposits across the Cretaceous Interior Seaway of North America, *Kaufmann* [1988] described five major tectonic features, with the active Cordilleran margin to the west. These include (from west to east): foredeep basin; linear forebulge zone; deep marine axial basin; tectonically active eastern hinge zone characterized by small, intermittently active horsts and grabens; and a shallow cratonic platform. In the Western Canada Sedimentary Basin (WCSB), the area of the central Saskatchewan kimberlite field is referred to as the East Median Hinge Zone [*Stott et al.*, 1993]. Clusters of kimberlites in central Saskatchewan exhibit strong linear trends at 305° and 335° (supporting information S1) that are coincident with the trace of the axial plane of the WCSB. Larger kimberlite bodies with multiple diatremes/feeder-vents show a similar alignment of individual diatremes along an azimuth of 305° (e.g., Orion South) [*Kjarsgaard et al.*, 2009a]. Detailed regional Cretaceous stratigraphic sections across the Fort à la Corne 'main kimberlite trend' indicate this area was a localized, linear topographic high (a horst block) during the mid-Cretaceous [*Kjarsgaard et al.*, 2001], consistent with the ideas of *Kaufmann* [1988].

Figure 5. Somerset Island, central Saskatchewan, and Kansas kimberlite tracer isotopic data. (a) $^{87}Sr/^{86}Sr(i)$ versus εNd(i). Whole rock data: Saskatchewan, filled red squares (this study; *Hegner et al.* [1995]); Somerset Island, filled green squares (this study; *Schmidberger et al.*, [2001]); Kansas = filled blue squares [*Alibert and Albarède*, 1988]. Range of least radiogenic TIMS $^{87}Sr/^{86}Sr(i)$ from perovskite for Somerset Island and Saskatchewan kimberlite samples shown as horizontal bars. Somerset Island perovskite Sr and whole rock Nd isotopic data, filled green diamonds (this study). Somerset Island perovskite isotopic data for Sr and Nd via LA-MC-ICPMS and LA-ICPMS, respectively, is shown as open green diamonds (data of *Wu et al.* [2010, 2013]). (b) The Somerset and Saskatchewan Sr-Nd boxes are defined by perovskite initial Sr with whole rock or perovskite Nd isotopic data (see Figure 5a). Kansas Sr-Nd box defined by initial Sr from the phlogopite isochron of *Blackburn et al.* [2008] with the whole rock εNd(i) from *Alibert and Albarède* [1988]. Nd-Sr data from perovskite separates for Chidliak, Baffin Island [*Heaman et al.*, 2015] and Eastern North America [*Zurevinski et al.*, 2011] are shown for comparison. The Jericho [*Dowall*, 2004] and Lac de Gras [*Dowall*, 2004; *Tappe et al.*, 2013] data are from whole rock powders, with the four individual Lac de Gras data points (small boxes) utilizing perovskite initial Sr [*Sarkar et al.*, 2015] combined with the whole rock εNd(i) data. Data for South African Group I kimberlites within the age range 120–80 Ma are from TIMS perovskite [*Heaman*, 1989] LA-MC-ICPMS perovskite [*Griffin et al.*, 2014, and references therein], and combined LA-MC-ICPMS (Sr) and LA-ICPMS (Nd) perovskite [*Wu et al.*, 2010, 2103]. Two data points from the *Griffin et al.* [2014] data set from Gope 25 (0.70314, −3.7) and Goedehoop (0.70384, +18.1) lie well outside the OIB array and the field for southern African Gp I kimberlites and are not considered further. (c) εNd(i) versus εHf(i). Whole rock data for Somerset Island (green filled circles) and Saskatchewan (filled red circles) are from this study. Whole rock data for Lac de Gras kimberlites are from *Dowall* [2004] and *Tappe et al.* [2013], Jericho from *Dowall* [2004], and South Africa from *Nowell et al.* [2004]. The Hf-Nd mantle array is after *Chauvel et al.* [2008].
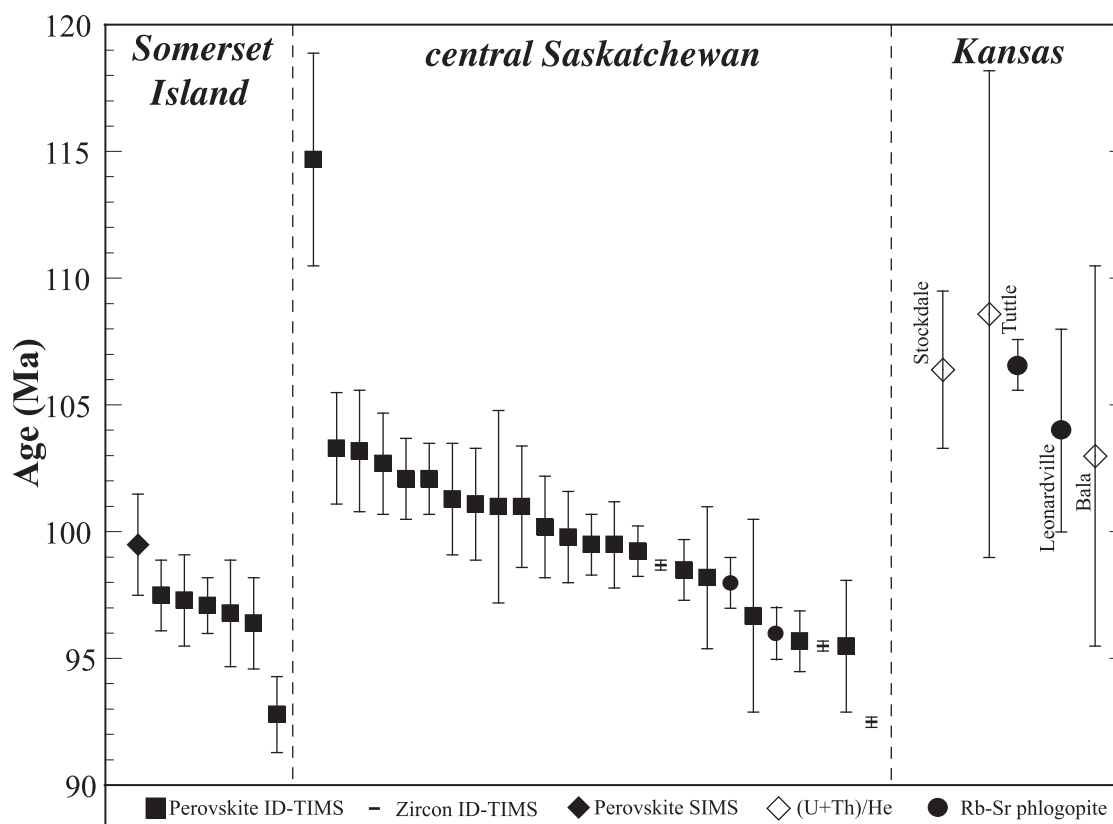
Figure 6. Central North America, mid-Cretaceous kimberlite age compilation. Only the preferred or best age (with 2σ uncertainty), for any individual kimberlite is plotted, unless there are multiple defined events at a single kimberlite body. See text for sources of data.

In Kansas, the kimberlites are emplaced through the subsurface extension of the 1.1 Ga Midcontinent Rift system [*Cullers et al.*, 2012]. In detail, the kimberlites are located on the east flank of the Abilene Anticline, recognized in Permian rocks as a horst and graben feature [*Berendsen*, 1997]. The Humboldt fault zone further to the east demarcates the eastern margin of the Midcontinent Rift system. Crustal lithologies include 800 m of Ordovician to Permian strata, which overlie Midcontinent Rift basin arkosic sediment in-fill and basic lava flows plus intrusions [*Cullers et al.*, 2012]. Precambrian structures include rift-related NNE trending faults, and orthogonal NW trending faults, with both fault sets being reactivated throughout time [*Berendsen*, 1997]. Detailed geophysical surveys indicate the kimberlites are controlled or influenced by faults associated with the Midcontinent Rift, and there is both recent and historical earthquake activity associated with these faults [*Steeples et al.*, 1987]. During mid-Cretaceous time, this area of Kansas was structurally active [*Bunker et al.*, 1988], and is equivalent to central Saskatchewan in that it is part of the eastern hinge zone of the Cretaceous interior basin.

We therefore suggest that the Kansas and Saskatchewan kimberlites were in a similar tectonic environment—the eastern hinge zone of the interior basin at mid-Cretaceous time—and that basin sedimentation, far-field Cordilleran tectonics, and Farallon slab influence [e.g., *Spasojevic et al.*, 2009; *Currie and Beaumont*, 2011], resulted in horst and graben structures via reactivation of older faults, that allowed for ascent and emplacement of small volume kimberlite magmas. Other types of magmatism (e.g., basalt or carbonatite) are not known to be spatially or temporally affiliated with the Saskatchewan kimberlite field. The Kansas kimberlites are slightly older or coeval with lamproites (southern Kansas and Arkansas) and alkali-silicate-carbonatite magmatism (e.g., Magnet Cove, Arkansas); these alkaline rocks are spatially associated within the extensive late Precambrian-Cambrian failed paleorift system [*Phipps*, 1988].

5.3. Tracer Isotope Perspectives on Mid-Cretaceous Kimberlites
Our new whole rock and perovskite isotopic results, combined with published data (Figures 4a, 4b, 5a–5c), illustrate that a combination of perovskite Sr with whole rock Nd-Hf isotopic information provides a robust

data set that is minimally affected by crustal contamination and postemplacement alteration processes. The least contaminated mid-Cretaceous Somerset Island, central Saskatchewan, and Kansas kimberlites have remarkably similar, Bulk Earth-like Sr-Nd-Hf isotopic compositions (Figures 5a–5c). Furthermore, these kimberlites are isotopically distinct from other studied North American kimberlites (Figures 5b and 5c), such as the Late Cretaceous to Paleogene Lac de Gras kimberlites [*Dowall*, 2004; *Tappe et al.*, 2013; *Sarkar et al.*, 2015], the Triassic to Early Cretaceous kimberlites in eastern North America [*Zurevinski et al.*, 2011], the Jurassic Chidliak field on Baffin Island [*Heaman et al.*, 2015], and the Jurassic Jericho kimberlite cluster on the Slave craton [*Dowall*, 2004].

The different lithospheric blocks underpinning the kimberlites of Somerset Island (Archean northern Rae domain of the Churchill Province), central Saskatchewan (Archean Sask Craton) and Kansas (Mesoproterozoic Yavapai terrane), make it highly unlikely that their very uniform yet highly distinctive isotopic signature is due to lithospheric mantle contamination. The isotopic coherence shown by these kimberlites along a >4000 km corridor, across such a geologically and geographically diverse region, when viewed in the context of near-identical emplacement ages, points to a common, deep mantle source for kimberlite in these three fields, which cannot be from highly depleted material in the upper asthenosphere. As the Sr-Nd-Hf isotopic signature of these kimberlites falls squarely within the OIB field, potential source regions would include the transition zone, adjacent lower mantle, or nondepleted asthenosphere. The Sr-Nd isotopic compositions of North American (this study) and southern African Group 1 kimberlites emplaced within the 120–80 Ma time interval (Figure 5b) do not overlap, suggesting there is no relationship between these North American and African kimberlites, consistent with spatial imaging of the African LLSVP and associated plumes [*Torsvik et al.*, 2010].

5.4. Geodynamic Processes and Magmatic Triggers
5.4.1. On the Absence of Mantle Plumes
The spatial and temporal coincidence of Mesozoic kimberlites in Africa and plume generation zones at the margins of the African large low-shear wave velocity province (LLSVP) where described by *Torsvik et al.* [2010]. At mid-Cretaceous time, the central North American kimberlite corridor lies >1500 km to the west of the western edge of the African LLSVP and cannot be related to this feature [*Currie and Beaumont*, 2011]. More recently, *Torsvik et al.* [2016] concluded that mid-Cretaceous North American kimberlites are not sourced from plumes from the deep mantle, as global tomography illustrates this region is cold and of high velocity. Somerset Island kimberlites are not related to the proposed high Arctic large igneous province (HALIP) plume head (initiated at 130 Ma); it is too old in relation to the kimberlite ages (97–93 Ma) and 1200 km distal (Figure 1). We conclude that the mid-Cretaceous North American kimberlite corridor does not appear to correspond to any known mantle plumes or plume hotspot tracks.
5.4.2. The Farallon Slab, Revisited
The mid-Cretaceous kimberlite corridor parallels the convergent western margin of North America (Figure 1) and the subducting Farallon slab, as previously noted by *Sharp* [1974], *McCandless* [1999], *Heaman et al.* [2003], *Currie and Beaumont* [2011], and *Duke et al.* [2014]. In the *McCandless* [1999] model, the general age progression of Jurassic (eastern), Cretaceous (central), and Eocene (western) kimberlites across North America (see Figure 1) is interpreted to be a consequence of a westward younging temporal release of slab-derived fluids, which initiates melt generation. The *Currie and Beaumont* [2011] model for kimberlite generation is similar, with fluid release from the slab and subsequent kimberlite melt generation. In both these models, kimberlite melt generation occurs in the upper asthenosphere, initiated by slab-derived fluids. However, if kimberlites are subduction related they should exhibit a diagnostic subduction trace element signature e.g., a negative Nb-Ta anomaly, which is not observed. *Duke et al.* [2014] examined a wide variety of Cretaceous to Eocene rock types (kimberlite, alkali silicate-carbonatite, lamproite, etc.) across continental U.S., between Arkansas and Montana. They suggested the 110–94 Ma magmatism in Arkansas and Kansas resulted from asthenospheric upflow associated with the eastern edge of the Farallon slab, facilitated by "tears" in the slab.

Geophysical studies of the mantle below the United States have imaged high velocity anomalies at depth [e.g., *Bunge and Grand*, 2000; *Sigloch et al.*, 2008], which represents the present-day location of the Farallon slab, interpreted to have extended from the Canadian Arctic Islands to the southern U.S. [*Spasojevic et al.*, 2009; *Shephard et al.*, 2014]. *Liu et al.* [2008] and *Spasojevic et al.* [2009] reconstructed the Farallon slab back to mid-Cretaceous time using present-day seismic tomography with temporal evolution (plate motion) and

stratigraphic constraints (paleoshorelines, tectonic subsidence, sediment isopachs) for the United States and southern Canada. Based on this study, the leading (eastern) edge of the eastward subducting Farallon slab corrected for plate motion to ∼100 Ma lies just to the west of Saskatchewan kimberlite field, but lies ∼1200 km west of the Kansas kimberlite field (Figures 1 and 7a). The Farallon slab at ∼100 Ma is modeled to have just penetrated through the transition zone into the lower mantle (Figure 7a) [*Liu et al.*, 2008; *Spasojevic et al.*, 2009]. We thus suggest that previous models invoking a relationship between kimberlites in central and eastern U.S and the Farallon slab are not consistent from a temporal and 3-D spatial perspective.
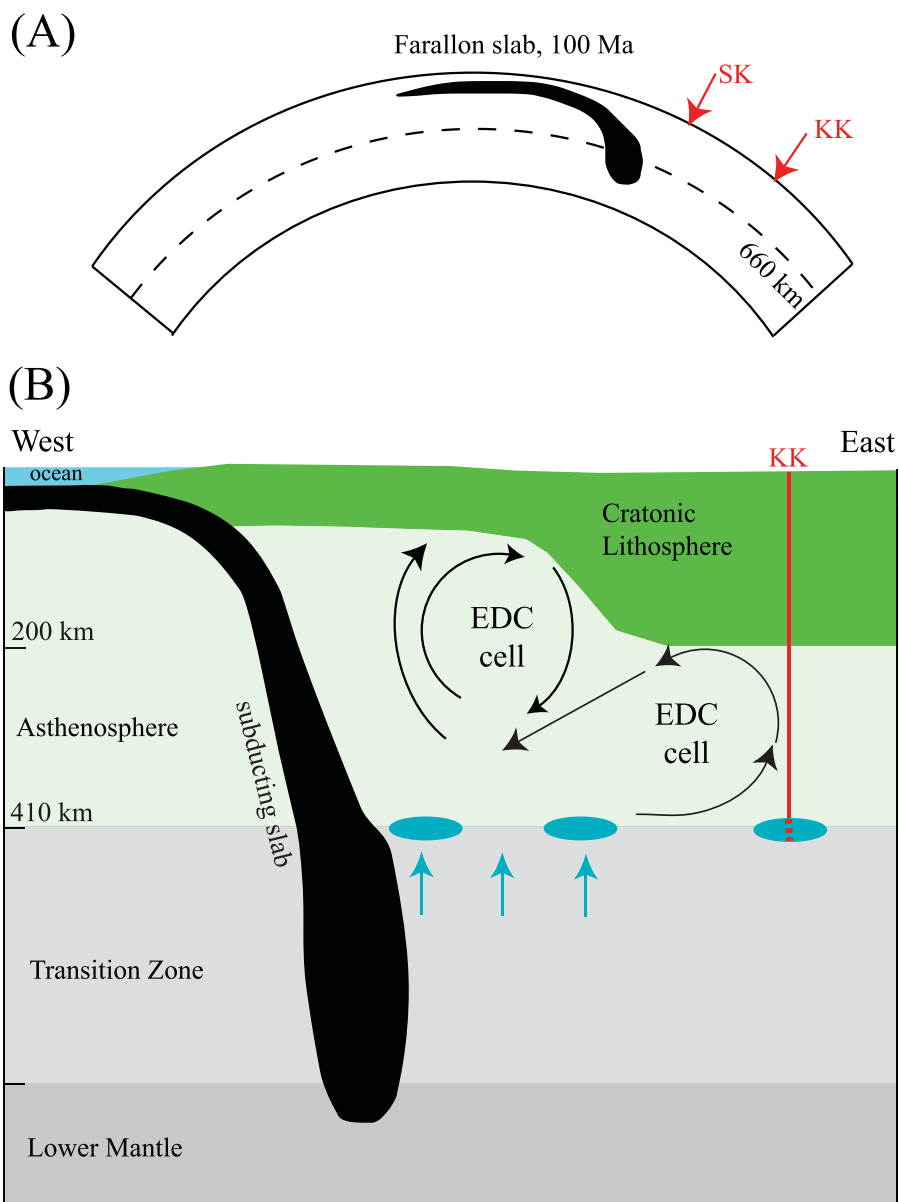

Figure 7. (a) Farallon slab cross section, 41° N, at 100 Ma (after *Liu et al.*, 2008; *Spasojevic et al.*, 2009], illustrating the spatial relationship between the Farallon slab and the Kansas kimberlite (KK) field. The relationship of the Farallon slab and the Saskatchewan kimberlite (SK) field is also shown, but this is based on the plan view geometry as shown in Figure 1. (b) Interpreted cross-section illustrating the influence of an edge-driven convection cell at an attenuated lithosphere margin, and melt generation and transport for Kansas kimberlites (KK). Thin black arrows represent asthenosphere convection associated with the EDC cell. Thick-dashed red line represents kimberlite melt generation in the lowermost asthenosphere or within the upper transition zone; thin red line is kimberlite ascent path to the surface. Blue ovals are water-rich zones at the top of the transition zone. The thin blue arrows in the transition zone represent water release from a locally thickened transition zone, after thermal equilibration of the cold Farallon slab.

5.4.3. Edge-Driven Convection

The single commonality of the three mid-Cretaceous kimberlite fields is they are all adjacent to the North American cratonic margin (Figure 1) [*Schaeffer and Lebedev*, 2014], where there is dramatic lithospheric thinning towards Mesozoic basins. *McKenzie and Priestly* [2008] have previously documented kimberlites occurring in regions of lithospheric thickness gradients. Recent USArray data have delineated a sharp boundary between a deep (and strong) versus a shallow (and weak) lithosphere-asthenosphere boundary west of the Kansas kimberlite field [*Foster et al.*, 2013]. Such a strong lithospheric gradient, coupled with the thermal blanketing effect of the very large North American cratonic mass could be conducive to the formation of an edge-driven convection (EDC) cell [e.g., *Elder*, 1976; *King and Anderson*, 1998].

EDC mantle upwelling and resulting magmatism is focused within the attenuated lithospheric section of the EDC cell. Magmas generated by EDC processes are not kimberlitic, but typically of basaltic to alkali basaltic composition, with melt sources in the upper asthenosphere and/or lower lithospheric mantle [*Kaislaniemi and van Hunen*, 2014; *Rudzitis et al.*, 2016]. However, the EDC modeling by *Kaislaniemi and van Hunen* [2014, Figure 4] also illustrates there is an associated (but less intense) mantle upwelling under the thick lithosphere, 200–300 km back from the attenuated lithosphere edge, as shown in Figure 7b. We suggest that EDC processes are the top-driven mechanism that facilitates decompression melting and upward migration of kimberlite magma from deep in the mantle. Consistent with the notion of mid-Cretaceous EDC related magmatism is the occurrence of lamproites at Prairie Creek, which are associated with the attenuated part of the lithosphere, and melting of SCLM.

5.4.4. An Integrated Geochemical, Geophysical, and Tectonic Model

In order to fulfill the requirement of generating, isotopically OIB-like, similar CO_2 and H_2O-rich kimberlite melts that erupt over a geographically widespread area in a variety of different tectonic settings, we suggest the source region is within the upper transition zone, or in the asthenospheric mantle just above the transition zone (Figures 7b and 8). What triggers the magma generation process? The most plausible explanation is water-fluxed decompression melting, facilitated by EDC processes. The decompression of hydrous ringwoodite [*Pearson et al.*, 2014] or wadsleyite to a lower pressure regime will release H_2O due to the negative slope of the ringwoodite to wadsleyite, and wadsleyite to olivine phase transitions in P-T space (Figure 8), as bulk H_2O concentration exceeds upper mantle peridotite storage capacity [*Tenner et al.*, 2012]. Seismic detection of a low velocity feature at the top of the transition zone supports an hypothesis of incipient melting produced by water exsolution from transition zone phases, with these melts interpreted to be sporadic and laterally discontinuous beneath North America [*Schmandt et al.*, 2011] and globally [*Tauzin et al.*, 2010]. With respect to a cold Farallon slab in the transition zone (Figures 7a and 7b), it will thicken the transition zone, but as it thermally equilibrates (with a delayed response time), the H_2O solubility in wadsleyite and ringwoodite decreases with increasing temperature [*Keppler and Bolfan-Casanova*, 2006], releasing water. This slab specific H_2O-release mechanism is suggested as applicable to the Saskatchewan kimberlite field, due to its spatial proximity to the Farallon slab at ~100 Ma (Figures 1 and 7), and could explain the high volume of kimberlite observed in Fort à la Corne, Saskatchewan, as compared to Somerset Island or Kansas.

The upper mantle has low concentration levels of CO_2 [*Dasgupta and Hirschmann*, 2007, and references therein], but the presence of superdeep diamond inclusions, crystallized from primitive carbonatitic melts in the transition zone/lower mantle, supports the notion of CO_2-rich melts at these depths [*Walter et al.*, 2008]. Hence low degrees of partial melting of the transition zone or lowermost asthenosphere with the water flux will generate a H_2O and CO_2-rich protokimberlite melt. That kimberlite melts have high water contents (in addition to high CO_2) is confirmed via experiments [*Edgar et al.*, 1988; *Mousallam et al.*, 2016] and whole rock studies on ultrafresh hypabyssal kimberlites [*Kjarsgaard et al.*, 2009b]. This kimberlite melting model is a variation on the concept of *Bercovici and Karato* [2003], which proposed ambient lower mantle upwelling through the transition zone with hydrous melts forming at the top of the transition zone (410 km), with these melts (basaltic in their model) interpreted to be dense and not buoyant. We interpret that a volatile-rich kimberlite melt (in contrast to a wet basaltic melt) is intrinsically buoyant [e.g., *Wilson and Head*, 2007].

In North America, mid-Cretaceous kimberlites are observed in regions with deep-seated major lithospheric structures that are reactivated at this time, which allows for passage of these small volume melts. A corollary is the potential of failed kimberlites that could not traverse the lithosphere due to an absence of deep-seated structures. All three kimberlite fields are intimately associated with major structures: Somerset Island
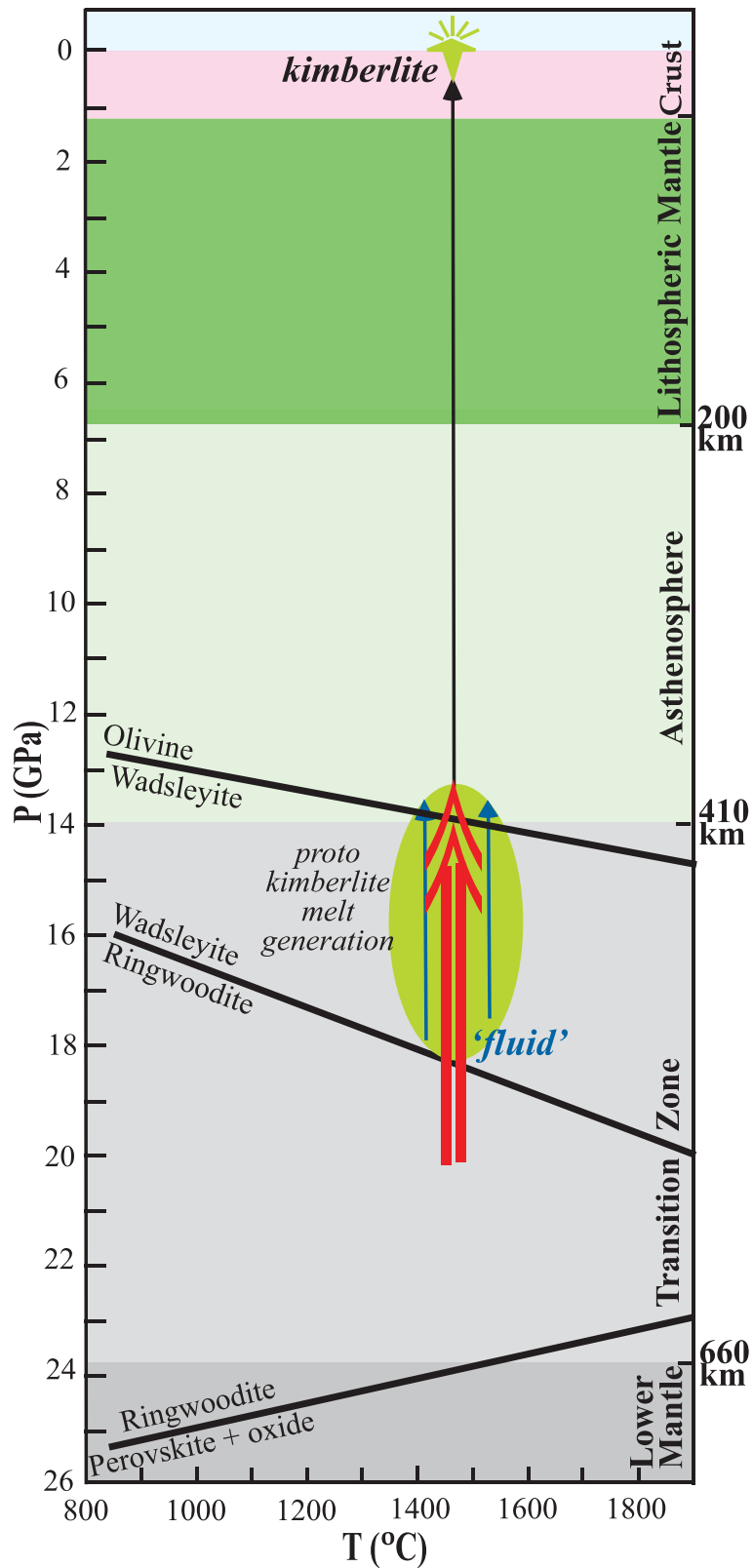
Figure 8. Pressure-temperature cross section of the Earth to ∼700 km depth, with stability fields [after *Litasov and Ohtani*, 2005] for olivine and its polymorphs (wadsleyite, ringwoodite, perovskite + oxide), in the transition zone. Decompression from upflow will cause ringwoodite or wadsleyite to invert and release water, which metasomatises the uppermost transition zone or lowermost part of the asthenosphere containing C-O-H-bearing peridotite, resulting in the generation of kimberlite melt.

kimberlites are adjacent to the Thelon tectonic zone, Saskatchewan kimberlites to the Sask Craton/Trans Hudson Orogen boundary, and Kansas kimberlites are within the Midcontinent Rift (Figure 1). Given the isotopic constraints imposed by our sample suite, there is no obvious or significant input from older recycled oceanic crust stored in the transition zone, nor do we see any significant modification en-route via interaction with depleted asthenosphere, or with lithospheric mantle or crust. We recognize that the isotopic signatures of the kimberlites considered here do not uniquely constrain the geodynamic model proposed above, but posit that this model is best able to satisfy the combination of geochemical parameters, and temporal, geographic, and tectonic constraints.

An examination of North American kimberlites within a tectonic and geodynamic context indicates a significant diversity in tectonic settings and chronology that ranges from: (1) Mesozoic kimberlite magmatism on the continental extension of Great Meteor hotspot track [*Heaman and Kjarsgaard*, 2000; *Zurevinski et al.*, 2011]; (2) Jurassic kimberlite magmatism (Chidliak) related to early initiation of the Labrador Sea basin (upwelling asthenosphere, lithosphere extension, continental rifting), on the margin of the African LLSVP [*Heaman et al.*, 2015]; (3) Mid-Cretaceous kimberlite magmatism inboard of the attenuated North American craton margin related to EDC processes and wet decompression melting (this study); and, (4) Late Cretaceous to Paleogene Lac de Gras kimberlites generated by vigorous return mantle flow related to fast and complex subduction [*Tappe et al.*, 2013]. Thus in North America it appears that the known kimberlites are not all related to the exact same mantle processes, and we suggest this is likely true for kimberlites from a global perspective when examined in detail.

6. Conclusions

We identify and characterize a >4000 km long corridor of approximately synchronous, isotopically similar mid-Cretaceous kimberlite magmatism in central North America. The known magmatism occurs in three widely separated kimberlite fields; the main periods of magmatism are 97–92 Ma Somerset Island, 103–96 Ma Central Saskatchewan, and 109–103 Ma in Kansas. Source region Sr-Nd-Hf isotope homogeneity indicates an ultradeep asthenospheric or transition zone Bulk Earth-like OIB source for these kimberlites. Our preferred explanation of the temporal, spatial, and chemical characteristics of these magmas is their generation via the initiation of partial melting to form volatile-rich kimberlite magma due to water-fluxed decompression melting of C-O-H-bearing peridotite in the transition zone, or the overlying asthenosphere. The driver for this process is mantle upflow facilitated by top-driven, EDC processes. "Shallow" lithospheric processes control the locus of kimberlite volcanism in the crust, explaining the disparate geographic nature of the erupted magmas.

References

Alibert, C., and F. Albarède (1988), Relationships between mineralogical, chemical and isotopic properties of some North American kimberlites, *J. Geophys. Res.*, *93*, 7643–7671, doi:10.1029/JB093iB07p07643.

Ashton, K. E., L. M., Heaman, J. F. Lewry, R. P. Hartlaub, and R. Shi (1999), Age and origin of the Jan Lake Complex: A glimpse at the buried Archean craton of the Trans-Hudson Orogen, *Can. J. Earth Sci.*, *36*, 185–208.

Aspler, L., and J. R. Chiarenzelli (1998), Two Neoarchean supercontinents? Evidence from the Paleoproterozoic, *Sediment Geol.*, *120*, 75–104.

Baksi, A. K. (1999), The timing of late Cretaceous alkalic igneous activity in the northern Gulf of Mexico, *J. Geol.*, *105*, 629–643.

Bell, K., and J. Blenkinsop (1987), Nd and Sr isotopic compositions of East African carbonatites: Implications for mantle heterogeneity, *Geology*, *15*, 99–102.

Bercovici, D., and S. Karato (2003), Whole-mantle convection and the transition-zone water filter, *Nature*, *425*, 39–44, doi:10.1038/nature01918.

Berendsen, P. (1997), Tectonic evolution of the Midcontinent Rift system in Kansas, in *Middle Proterozoic to Cambrian Rifting, Central North America*, *Geol. Soc. Am. Spec. Pap.*, vol. 312, edited by R. W. Ojakangas et al., pp. 235–242, Geol. Soc. Am., Boulder, Colo.

Berryman, A., B. H. Scott Smith, and B. Jellicoe (2004), Geology and diamond distribution of the 140/141 kimberlite, Fort à la Corne, central Saskatchewan, Canada, *Lithos*, *76*, 99–114.

Blackburn, T. J., D. F. Stockli, R. W. Carlson, and P. Berendsen (2008), (U-Th)/He dating of kimberlites: A case study from north-east Kansas, *Earth Planet. Sci. Lett.*, *275*, 111–120, doi:10.1016/j.epsl.2008.08.006.

Blichert-Toft, J., and F. Albarède (1997), The Lu-Hf isotope geochemistry of chondrites and the evolution of the mantle-crust system, *Earth Planet. Sci. Lett.*, *148*, 243–258.

Buchan, K., and R. Ernst (2006), Giant dyke swarms and reconstruction of the Canadian Arctic Islands, Greenland, Svalbard and Franz Josef Land, in *Proceedings of the 5th International Dyke Conference*, edited by E. Hanski et al. pp. 27–48, Taylor and Francis, London, U. K.

Bunge, H. P., and S. P. Grand (2000), Mesozoic plate-motion history below the northeast pacific Ocean from seismic images of the subducted Farallon slab, *Nature*, *405*, 337–340, doi:10.1038/35012586.

Bunker, B. J., B. J. Witzke, W. L. Watney, and G. A. Ludvigson (1988), Phanerozoic history of the central midcontinent, United States, in *Sedimentary Cover of the North American craton, Geology of North America* vol. 2, pp. 243–260, edited by L. L. Sloss, Geol. Soc. Am., Boulder, Colo.

Chauvel, C., E. Lewin, M. Carpentier, N. T. Arndt, and J. C. Marini (2008), Role of recycled oceanic basalt and sediment in generating the Hf–Nd mantle array, *Nat. Geosci.*, *1*, 64–67, doi:10.1016/j.epsl.2010.12.036.

Chiarenzelli, J. R. (1989), The Nistowiak and Guncoat Gneisses: Implications for the tectonics of the Glennie and la Ronge domains, northern Saskatchewan, Canada, PhD thesis, Univ. of Kans., Kansas City.

Clement, C. R. (1982), A comparative geological study of some major kimberlite pipes in the Northern Cape and Orange Free State, PhD thesis, Univ. of Cape Town, Cape Town, S. Afr.

Clement, C. R., E. M. W. Skinner, and B. H. Scott Smith (1984), Kimberlite re-defined, *J. Geol.*, *32*, 223–228.

Cox, R. A., and D. H. C. Wilton (2006), UP–Pb dating of perovskite by LA-ICPMS: An example from the Oka carbonatite, Quebec, Canada, *Chem. Geol.*, *235*, 21–32, doi:10.1016/j.chemgeo.2006.06.002.

Crough, S. T., W. J. Morgan, and R. B. Hargraves (1980), Kimberlites: Their relation to mantle hotspots, *Earth Planet. Sci. Lett.*, *50*, 260–274.

Cullers, R. L., P. Berendsen, and A. Barczuk (2012), The geology, petrology, and elemental composition of kimberlites from Riley and Marshall Counties, Kansas, USA, *Kans. Geol. Surv. Open File Rep. 2012–17*, 41 pp.

Currie, C. A., and C. Beaumont (2011), Are diamond-bearing cretaceous kimberlites related to low-angle subduction beneath western North America?, *Earth Planet. Sci. Lett.*, *303*, 59–70, doi:10.1016/j.epsl.2010.12.036.

Dasgupta, R., and M. M. Hirschmann (2007), Effect of variable carbonate concentration on the solidus of mantle peridotite, *Am. Mineral.*, *92*, 370–379, doi:10.2138/am.2007.2201.

Davis, W. J., R. A. Stern, and B. A. Kjarsgaard (1998), Geochronology of crustal xenoliths from Saskatchewan kimberlites; A glimpse at the buried Trans-Hudson Orogen, in *Geological Society of America Annual Meeting, Geol. Soc. Am. Abstr. Programs*, *30*(7), 110 pp.

Dowall, D. P. (2004), Elemental and isotopic geochemistry of kimberlites from the Lac de Gras field, Northwest Territories, Canada, PhD thesis, Durham Univ., Durham, U. K.

Duke, G. I., R. W. Carlson, C. D. Frost, B. C. Hearn Jr., and G. N. Eby (2014), Continent-scale linearity of kimberlite-carbonatite magmatism, mid-continent North America, *Earth Planet. Sci. Lett. 403*, 1–14, doi:10.1016/j.epsl.2014.06.023.

Eby, G. N., and P. Vasconcelos, (2009), Geochronology of the Arkansas alkaline province, southeastern United States, *J. Geol.*, *117*, 615–626, doi:10.1086/605779.

Eccles, D. R., R. A. Creaser, L. M. Heaman, and J. Ward (2008), Rb-Sr and U-Pb geochronology and setting of the Buffalo Head Hills kimberlite field, northern Alberta, *Can. J. Earth Sci.*, *45*, 513–529, doi:10.1038/35012586

Edgar, A. D., M. Arima, D. K. Baldwin, D. R. Bell, S. R. Shee, E. M. W. Skinner, and E. C. Walker (1988), High pressure–high temperature melting experiments on a SiO_2-poor, CaO-rich aphanitic kimberlite from the Wesselton mine, Kimberley, South Africa, *Am. Mineral*, *73*, 524–533.

Elder, J. (1976), *The Bowels of the Earth*, Oxford Univ. Press, Oxford, U. K.

Embry, A., and B. Beauchamp (2009), Sverdrup Basin, in *Sedimentary Basins of the World*, vol. 5, edited by A.D. Miall, pp. 451–471, Elsevier, Amsterdam. doi:10.1016/51874-5997(08)00013-0.

Embry, A., and J. Dixon (2000), The breakup unconformity of the Amerasia Basin, Arctic Ocean: Evidence from Arctic Canada, *Geol. Soc. Am. Bull.*, *102*, 1526–1534.

Fipke, C. E., J. J. Gurney, and R. O. Moore (1995), Diamond exploration techniques emphasizing indicator mineral geochemistry and Canadian examples, *Geol. Surv. Can., Bull.*, *423*, 86 pp.

Foster, K., K. Dueker, B. Schmandt, and H. Yuan (2013), A sharp cratonic lithosphere-asthenosphere boundary beneath the American Midwest and its relation to mantle flow, *Earth Planet. Sci. Lett.*, *402*, 82–89, doi:10.1016/j.epsl.2013.11.018

Gogenini, S. V., C. E. Melton, and A. A. Giardini (1978), Some petrological aspects of the Prairie Creek diamond-bearing kimberlite diatreme, Arkansas, *Contrib. Mineral Petrol.*, *66*, 251–261.

Goldstein, S. L., R. K. O'Nions, and P. J. Hamilton (1984), A Sm-Nd study of atmospheric dusts and particulates from major river systems, *Earth Planet Sci. Lett.*, *70*, 221–236.

Gradstein, F. M., J. G. Ogg, M. D. Schmitz, and M. D. Ogg (2012), *The Geologic Time Scale 2012*, Elsevier, Amsterdam.

Griffin, W. L., N. J. Pearson, E. Belousova, S. E. Jackson, E. van Achterbergh, S. Y. O'Reilly, and S. R. Shee (2000), The Hf isotope composition of cratonic mantle: LAM-MC-ICPMS analysis of zircon megacrysts in kimberlites, *Geochim. Cosmochim. Acta*, *64*, 133–147, doi:10.1016/S0016-7037(99)00343-9.

Griffin, W. L., J. M. Batumike, Y. Greau, N. J. Pearson, S. R. Shee, and S. Y. O'Reilly (2014), Emplacement ages and sources of kimberlites and related rocks in southern Africa: U–Pb ages and Sr–Nd isotopes of groundmass perovskite, *Contrib. Mineral. Petrol.*, *168*(1032), 13 pp., doi:10.1086/605779.

Grunsky, E. C., and B. A. Kjarsgaard (2008), Classification of eruptive phases of the Star Kimberlite, Saskatchewan, Canada based on statistical treatment of whole-rock geochemical analyses, *Appl. Geochem.*, *23*, 3321–3336.

Haggerty, S. E. (1982), Kimberlites in western Liberia: An overview of the geological setting in a plate tectonic framework, *J. Geophys. Res.*, *87*, 10,811–10,826, doi:10.1029/JB087iB13p10811.

Haggerty, S. E. (1994), Superkimberlites: A geodynamic window to the Earth's core, *Earth Planet. Sci. Lett.*, *122*, 57–69

Harvey, S., B. A. Kjarsgaard, M. McClintock, M. Shimmell, L. Fourie, P. Du Plessis, and G. Read (2009), Geology and evaluation strategy of the Star and Orion South kimberlite, Fort à la Corne, Canada, *Lithos*, *112*, 47–60

Heaman, L. M. (1989), The nature of the subcontinental mantle from Sr-Nd-Pb isotopic studies on kimberlitic perovskite, *Earth Planet. Sci. Lett.*, *92*, 323–334, doi:10.1016/0012-821X(89)90057-5.

Heaman, L. M., and B. A. Kjarsgaard (2000), Timing of eastern North American kimberlite magmatism: Continental extension of the Great Meteor hotspot track?, *Earth Planet. Sci. Lett.*, *178*, 253–268, doi:10.1016/S0012-821X(00)00079-0.

Heaman, L. M., B. A. Kjarsgaard, and R. A. Creaser (2003), The Timing of Kimberlite Magmatism in North America: Implications for Global Kimberlite Genesis and Diamond Exploration, *Lithos*, *71*, 153–184, doi:10.1016/j.lithos.2003.07.005.

Heaman, L. M., B. A. Kjarsgaard, and R. A. Creaser (2004), The temporal evolution of North American kimberlites, *Lithos*, *76*, 377–398, doi:10.1016/j.lithos.2004.03.047.

Heaman, L. M., J. Pell, H. Grutter, and R. A. Creaser (2015), U-Pb geochronology and Sr/Nd isotope composition of groundmass perovskite from the newly discovered Jurassic Chidliak kimberlite field, Baffin Island, Canada, *Earth Planet. Sci. Lett.*, *415*, 183–199, doi:10.1016/j.epsl.2014.12.056.

Hegner, E., J. C. Roddick, S. M. Fortier, and L. Hulbert (1995), Nd, Sr, Pb, Ar and O isotopic systematics of Sturgeon Lake kimberlite, Saskatchewan, Canada: Constraints on emplacement age, alteration and source composition, *Contrib. Mineral Petrol.*, *120*, 212–222.

Herrle, J. O., C. J. Schröder-Adams, W. Davis, A. T. Pugh, J. M. Galloway, and J. Fath (2015), Mid-Cretaceous High Arctic stratigraphy, climate, and oceanic anoxic events, *Geology*, *43*(5), 403–406, doi:10.1130/G36439.1.

Hofmann, A. W. (2014), Sampling mantle heterogeneity through oceanic basalts: Isotopes and trace elements, in *Treatise on Geochemistry*, 2nd ed., Elsevier, Amsterdam, doi:10.1016B978-0-08-095975-7.00203-5.

Horwitz, E. Ph., M. L. Dietz, and R. Chiarizia (1992), The application of novel extraction chromatographic materials to the characterization of radioactive waste solutions, *J. Radioanal. Nucl. Chem.*, *161*, 575–583.

Jaffey, A. H., K. F. Flynn, L. E. Glendenin, W. C. Bentley, and A. M. Essling (1971), Precision measurements of half-lives and specific activities of ^{235}U and ^{238}U, *Phys. Rev. C*, *4*, 1889–1906.

Janney, P. E., A. P. Le Roex, R. W. Carlson, and K. S. Viljoen (2002), A chemical and multi-isotope study of the Western Cape olivine melilitite province, South Africa: Implications for the sources of kimberlites and the origin of the HIMU signature in Africa, *J. Petrol.*, *43*, 2339–2370, doi:10.1038/324243a0.

Jelsma, H., W. Barnett, S. Richards, and G. Lister (2009), Tectonic setting of kimberlites, *Lithos*, *112S*, 155–165, doi:10.1016/j.lithos.2009.06.030.

Kaislaniemi, L., and J. van Hunen (2014), Dynamics of lithospheric thinning and mantle melting by edge-driven convection: Application to Moroccan Atlas Mountains, *Geochem. Geophys. Geosyst.*, *15*, 3175–3189, doi:10.1002/2014GC005414.

Kaufmann, E. G. (1988), Concepts and methods of high resolution event stratigraphy, *Annu. Rev. Earth Planet. Sci.*, *16*, 605–654, doi:10.1146/annurev.ea.16.050188.003133.

Keppler, H., and N. Bolfan-Casanova (2006), Thermodynamics of water solubility and partitioning, in *Water in Nominally Anhydrous Minerals*, Rev. Min. Geochem., vol. 62, edited by H. Keppler, and J. R.Smyth, pp. 193–220, Mineral. Soc. of Am., Chantilly.

King, S. D., and D. L. Anderson (1998), Edge-driven convection, *Earth Planet. Sci. Lett.*, *160*(3–4), 289–296, doi:10.1016/S0012-821X(98)00089-2.

Kinny, P. D., B. J. Griffin, L. M. Heaman, F. F. Brakhfogel, and Z. V. Spetsius (1997), SHRIMP U-Pb ages of perovskite from Yakutian kimberlites. *Russ. Geo. Geophys.*, *38*, 97–105.

Kjarsgaard, B. A. (1996a), Somerset Island kimberlite field, District of Franklin, Northwest Territories, *Geol. Surv. Can.*, *Open File Rep.*, *3228*, 61–66.

Kjarsgaard, B. A. (1996b), Prairie kimberlites, *Geol. Surv. Can. Open File Rep.*, *3228*, 67–72.

Kjarsgaard, B. A. (2007), Kimberlite diamond deposits, in *Mineral Deposits of Canada*, edited by W. Good fellow, Geol. Assoc. Can. Min. Dep. Div. Spec. Pub., *5*, pp. 245–272.

Kjarsgaard, B. A., and T. D. Peterson (1992), Kimberlite –derived ultramafic xenoliths from the diamond stability field: A new Cretaceous geotherm for Somerset Island, Northwest Territories, *Geol. Surv. Can. Curr. Res.*, *1992-B*, 1–6.

Kjarsgaard, B. A., D. A. Leckie, L. M. Heaman, D. McNeil, and D. McIntyre (2001), Cretaceous kimberlite chaos? Fort à la Corne revisited, reworked and resolved, *Summ. Invest. Sask. Geol. Surv. Misc. Rep.*, *2001–4.2*, 27–28.

Kjarsgaard, B. A., D. A. Leckie, and J. P. Zonneveld (2008), Geology and diamond distribution of the 140/141 kimberlite, Fort à la Corne, central Saskatchewan, *Lithos*, *97*, 422–428.

Kjarsgaard, B. A., S. Harvey, P. Du Plessis, M. McClintock, J. P. Zonneveld, L. M. Heaman, and D. McNeil (2009a), Geology of the Orion South Kimberlite, Fort à la Corne, Canada, *Lithos*, *112S*, 600–617, doi:10.1016/j.lithos.2009.06.001.

Kjarsgaard, B. A., D. G. Pearson, S. Tappe, G. M. Nowell, and D. P. Dowall (2009b), Geochemistry of hypabyssal kimberlites from Lac de Gras, Canada: Comparison to a global database and applications to the parent magma problem, *Lithos*, *112S*, 236–248, doi:10.1016/j.lithos.2009.05.039.

Kramers, J.D., and C.B. Smith (1983), A feasibility study of U-Pb and Pb-Pb dating of kimberlites using groundmass mineral fractions and whole-rock samples, *Chem. Geol.*, *1*, 23–38.

Leckie, D. A., B. A. Kjarsgaard, J. Bloch, D. McIntyre, D. McNeil, and L. Stasiuk (1997), Emplacement and re-working of diamond-bearing, crater-facies kimberlite in Albian sediments of central Saskatchewan, *Geol. Soc. Am. Bull.*, *109*, 1000–1024.

Lehnert-Theil, K., R. Loewer, R. G. Orr, and P. Robertshaw (1992), Diamond-bearing kimberlites in Saskatchewan, Canada: The Fort à la Corne case history, *Exp. Min. Geol.*, *1*, 391–403.

le Roex, A. P. (1986), Geochemical correlation between southern African kimberlites and South Atlantic hotspots, *Nature*, *324*, 243–245, doi:10.1038/324243a0.

le Roex, A. P., D. R. Bell, and P. Davis (2003), Petrogenesis of group I kimberlites from Kimberley, South Africa: Evidence from bulk-rock geochemistry, *J. Petrol.*, *44*, 2261–2286, doi:10.1093/petrology/egg077.

Litasov, K., and E. Ohtani (2005), Phase relations in hydrous MORB at 18–28 GPa: Implications for heterogeneity of the lower mantle, *Phys. Earth Planet. Int.*, *150*, 239–263, doi:10.1016/j.pepi.2004.10.010.

Liu, L., S. Spasojevic, and M. Gurnis (2008), Reconstructing Farallon plate subduction Beneath North America Back to the Late Cretaceous, *Science*, *322*, 934–938, doi:10.1126/science.1162921.

Lucas, S., A. Green, Z. Hajnal, D. White, J. Lewry, K. Ashton, W. Weber, and R. Clowes (1993), Deep seismic profile across a Proterozoic collision zone: Surprises at depth, *Nature*, *363*, 339–342.

Ludwig, K. R. (2003), *Isoplot/Ex v. 3.0: A Geochronological Toolkit for Microsoft Excel, Berkeley Geochron. Cent. Spec. Publ. 1a*, Berkeley Geochron. Cent., Berkeley, Calif.

Lugmair, G. W., and R. W. Carlson (1978), The Sm-Nd history of KREEP, *Lunar Planet. Sci. Conf. Proc.*, *9*, 689–704.

Malarkey, J., D. G. Pearson, B. A. Kjarsgaard, J. P. Davidson, G. M. Nowell, C. J. Ottley, and J. Stammer (2010), From source to crust: Tracing magmatic evolution in a kimberlite and a melilitite using microsample geochemistry, *Earth Planet. Sci. Lett.*, *299*, 80–90, doi:10.1016/j.epsl.2010.08.020.

McCandless, T. E. (1999), Kimberlites: Mantle expressions of deep-seated subduction, in *Proceedings of the 7th International Kimberlite Conference*, 2, edited by J. J. Gurney et al., pp. 545–549, Red Roof, Cape Town, S. Afr.

McKenzie, D., and K. Priestly (2008), The influence of lithospheric thickness variations on continental evolution, *Lithos*, *102*, 1–11.

McNeil, D. H., and G. Caldwell (1981), Cretaceous rocks and their foraminifera in the Manitoba Escarpment, *Geol. Assoc. Can. Spec. Pap.*, *21*, 439 pp.

McNeil, D. H., and C. F. Gilboy (2000), Cretaceous stratigraphy in four cores from the vicinity of the Fort à la Corne Kimberlite Field, east–central Saskatchewan: Preliminary results, *Sask. Geol. Surv. Misc. Rep.*, *2000–4.1*, 98–105.

Mitchell, R. H. (1975), Geology, magnetic expression and structural control of central Somerset Island kimberlites, *Can. J. Earth Sci.*, *12*, 757–764.

Mitchell, R. H. (1986), *Kimberlites*, Plenum, New York.

Mitchell, R. H. (1995), *Kimberlites, Orangeites and Related Rocks*, Plenum, New York, doi:10.1007/978-1-4615-1993-5.

Mitchell R. H., and D. B. Clarke (1976), Oxide and sulphide mineralogy of the Peuyuk kimberlite, Somerset Island, N.W.T., Canada, *Contrib. Mineral. Petrol.*, *56*, 157–172.

Mousallam, Y., Y. Morizet, and F. Gaillard (2016), H_2O-CO_2 solubility in low-SiO_2 melts and the unique mode of kimberlite degassing and emplacement, *Earth Planet. Sci. Lett.*, *299*, 151–160, doi:10.1016/j.epsl.2016.04.037.

Nixon, P. H. (1973), *Lesotho Kimberlites*, 350 pp., Lesotho Natl. Dev. Corp., Maseru, Lesotho.

Nowell, G. M., D. G. Pearson, D. R. Bell, R. W. Carlson, C. B. Smith, P. D. Kempton, and S. R. Noble (2004), Hf isotope systematics of kimberlites and their megacrysts: New constraints on their source regions, *J. Petrol.*, *45*, 1583–1612, doi:10.1086/605779.

Obradovich, J. D., T. Matsumoto, T. Nishida, T., and Y. Inoue (2002), Integrated biostratigraphic and radiometric scale on the Lower Cenomanian (Cretaceous) of Hokkaido, Japan, *Proc. Jpn. Acad. Ser. B, 78*(6), 149–153.

Ottley, C. J., D. G. Pearson, and G. J. Irvine (2003), A routine method for the dissolution of geological samples for the analysis of REE and trace elements via ICP-MS, in *Plasma source mass spectrometry – applications and emerging technologies*, edited by G. Holland et al., pp. 221–230, Royal Society of Chemistry, Cambridge, U. K.

Paton, C., J. M. Hergt, D. Phillips, J. D. Woodhead, and S. R. Shee (2007), New insights into the genesis of Indian kimberlites from the Dharwar Craton via in situ Sr isotope analysis of groundmass perovskite, *Geology, 35*, 1011–1014, doi:10.1130/G24040A.1.

Paton, C., J. M. Hergt, J. D. Woodhead, D. Phillips, and S. R. Shee (2009), Identifying the asthenospheric component of kimberlite magmas from the Dharwar craton, India, *Lithos, 112S*, 296–310, doi:10.1016/j.lithos.2009.03.019.

Pearson, D. G., and G. M. Nowell (2005), Accuracy and precision in plasma ionisation multi-collector mass spectrometry: Constraints from neodymium and hafnium isotope measurements, in *Plasma Source Mass Spectrometry*: Current Trends and Future Developments, edited by G. Holland, et al., pp. 284–314, Royal Society of Chemistry, Cambridge.

Pearson, D. G., et al. (2014), Hydrous mantle transition zone indicated by ringwoodite included within diamond, *Nature, 507*, 221–224, doi: 10.1038/nature13080.

Pell, J., H. Grenon, M. V. Sell, and L. Tam (2008), Exploration and discovery of a new kimberlite cluster on the Nanuq property, Western Churchill Province, Kivalliq area, Nunavut, in *9th International Kimberlite Conference, Frankfurt, Ext. Abs., 9IKC-A-00278*, 3 pp., Int. Kimb. Conf. Frankfurt.

Phipps, S. P. (1988), Deep rifts as sources for alkaline intraplate magmatism in eastern North America, *Nature, 334*, 27–31.

Ringwood, A. E., S. E. Kesson, W. Hibberson, and N. Ware (1992), Origin of kimberlites and related magmas, *Earth Plan. Sci. Lett., 113*, 521–538, doi:10.1016/0012-821X(92)90129-J.

Rudzitis, S., M.R. Reid, and J. Blichert-Toft (2016), On edge melting under the Colorado Plateau margin, *Geochem. Geophys. Geosyst., 17*, 2835–2854, doi:10.1002/2016GC006349.

Sarkar, C., C. D. Story, and C. J. Hawkesworth (2013), Detailed protracted crystallization history of perovskite in Orapa kimberlite, in *Proceedings of the 10th International Kimberlite Conference*, vol. 1, edited by D. G. Pearson et al. pp. 211–224, Springer, New Delhi.

Sarkar, C., C. D. Storey, and C. J. Hawkesworth (2014), Using perovskite to determine the pre-shallow level contamination magma characteristics of kimberlite, *Chem. Geol., 363*, 76–90, doi:10.1016/j.chemgeo.2013.10.032.

Sarkar, C., L. M. Heaman, and D. G. Pearson (2015), Duration and periodicity of kimberlite volcanic activity in the Lac de Gras kimberlite field, Canada and some recommendations for kimberlite geochronology, *Lithos, 218–219*, 155–166, doi:10.1016/j.lithos.2015.01.017.

Schaeffer, A. J., and S. Lebedev (2014), Imaging the North American continent using waveform inversion of global and USArray data, *Earth Planet. Sci. Lett., 402*, 26–41, doi:10.1016/j.epsl.2014.05.014.

Schmandt, B., K. G. Duecker, S. M. Hansen, J. J. Jasbinsek, and Z. Zhang (2011), A sporadic low-velocity layer atop the western US mantle transition zone and short wavelength variations in transition zone discontinuities, *Geochem. Geophys. Geosyst., 12*, Q08014, doi:10.1029/2011GC003668.

Schmidberger, S. S., A. Simonetti, and D. Francis (2001), Sr-Nd-Pb isotope systematics of mantle xenoliths from Somerset Island kimberlites: Evidence for lithosphere stratification beneath Arctic Canada, *Geochem. Cosmochem. Acta, 65*, 4243–4255, doi:10.1016/S0016-7037(01)00687-1.

Scott-Smith, B. H. (2008), The Fort à la Corne kimberlites, Saskatchewan, Canada: Geology, emplacement and economics, *J. Geol. Soc. India, 71*, 11–55.

Sharp, W. E. (1974), A plate tectonic origin for diamond-bearing kimberlite, *Earth Planet. Sci. Lett., 21*, 351–354, doi:10.1016/0012-821X(74)90173-3.

Shephard, G. E., N. Flament, S. Williams, M. Seton, M. Gurnis, and R. D. Müller (2014), Circum-Arctic mantle structure and long-wavelength topography since the Jurassic, *J. Geophys. Res. Solid Earth, 119*, 7889–7908, doi:10.1002/2014JB011078.

Sigloch, K., N, McQuarrie, and G. Nolet (2008), Two-stage subduction history under North America inferred from multiple-frequency tomography, *Nat. Geosci., 1*, 458–462, doi:10.1038/ngeo231.

Smith, C. B. (1983), Pb, Sr and Nd isotopic evidence for sources of southern African Cretaceous kimberlites, *Nature, 304*, 51–54, doi:10.1038/304051a0.

Smith, C. B., H. L. Allsopp, O. G. Garvie, J. D. Kramers, P. F. S. Jackson, and C. R. Clement (1989), Note on the U-Pb perovskite method for dating kimberlites: Examples from the Wesselton and DeBeers mines, South Africa, Somerset Island, Canada, *Chem. Geol., 79*, 137–145, doi: 10.1016/0168-9622(89)90016-X.

Spasojevic, S., L. Liu, and M. Gurnis (2009), Adjoint models of mantle convection with seismic, plate motion, and stratigraphic constraints: North America since the Late Cretaceous, *Geochem. Geophys. Geosyst., 10*, Q05W02, doi:10.1029/2008GC002345.

Steeples, D. W., G. M. Hildebrand, B. C. Bennett, R. D. Miller, Y. J. Chung, and R. W. Knapp (1987), Kansas-Nebraska seismicity studies using the Kansas-Nebraska micro-earthquake network, *Kan. Geol. Surv. Open File Rep., 1987–35*, 80 pp.

Stewart W. D. and J. W. Kerr (1987), Late Proterozoic to Early Tertiary stratigraphy of Somerset Island and northern Boothia Peninsula, District of Franklin, *Pap. Geol. Surv. Can., 83–26*, 78 p.

Stott, D. F., W. G. E. Caldwell, D. J. Cant, J. E. Christopher, J. Dixon, E. H. Koster, D. H. McNeil, and F. Simpson (1993), Cretaceous stratigraphy, in *Sedimentary Cover of the Craton in Canada*, edited by D.F. Stott et al., Geology of Canada, *Geol. Surv. Can., 5*, 358–438.

Sun, J., C. Z. Liua, S. Tappe, S. I. Kostrovitsky, F. Y. Wu, D. Yakovlev, Y. H. Yang, and J. H. Yang (2014), Repeated kimberlite magmatism beneath Yakutia and its relationship to Siberian flood volcanism: Insights from in-situ U-Pb and Sr-Nd perovskite isotope analysis, *Earth Planet. Sci. Lett., 404*, 283–295, doi:10.1016/j.epsl.2014.07.039.

Tainton, K., and D. McKenzie (1994), The generation of kimberlites, lamproites, and their source rocks, *J. Petrol., 35*, 787–817, doi:10.1093/petrology/35.3. 787.

Tappe, S., D. G. Pearson, B. A. Kjarsgaard, G. M. Nowell, and D. Dowall (2013), Mantle transition zone input to kimberlite magmatism near a subduction zone: Origin of anomalous Nd-Hf isotope systematics at Lac de Gras, Canada, *Earth Planet. Sci. Lett., 371–372*, 235–251, doi:10.1016/j.epsl.2013.03.039.

Tauzin, B., E. Debayle, and G. Wittlinger (2010), Seismic evidence for a global low velocity layer in the Earth's upper mantle, *Nat. Geocsi., 3*, 718–721, doi:10.1038/ngeo969.

Tenner, T. J., M. M. Hirschmann, A. C. Withers, and P. Ardia (2012), H_2O storage capacity of olivine and low-Ca pyroxene from 10 to 13 GPa: Consequences for dehydration melting above the transition zone, *Contrib. Mineral. Petrol., 163*, 297–316, doi:10.1007/s00410-011-0675-7.

Thirlwall, M. F. (1991), Long-term reproducibility of multicollector Sr and Nd isotope ratio analysis, *Chem. Geol., 94*(2), 85–104.

Torsvik, T. H., K. Burke, B. Steinberger, S. J. Webb, and L. D. Ashwal (2010), Diamonds sampled by plumes from the core–mantle boundary, *Nature, 466*, 352–355, doi:10.1038/nature09216.

Torsvik, T. H., B. Steinberger, L. D. Ashwal, P. V. Doubrovine, and R. G. Tronnes (2016), Earth evolution and dynamics: A tribute to Kevin Burke, *Can. J. Earth Sci.*, *53*, 1073–1087, doi:10.1139/cjes-2015-0228.

Trettin, H. P. (1991), Tectonic framework, in Geology of the Innuitian Orogen and Arctic Platform of Canada and Greenland, edited by H. P. Trettin, Geology of Canada, *Geol. Surv. Can.*, *3*, 59–66.

Villenueve, M. and M. C. Williamson (2006), ^{40}Ar-^{39}Ar dating of mafic magmatism from the Sverdrup Basin, in *Proceedings of the 4th Conference on Arctic Margins*, edited by R. A. Scott et al., pp. 206–215, US Dep. Int., Anchorage, Alaska.

Walter, M. J., et al. (2008), Primary carbonatitic melt from deeply subducted oceanic crust, *Nature*, *454*(7204), 622–625, doi:10.1038/nature07132.

Wagner, P. A. (1914), The Diamond Fields of South Africa, Transvaal Leader, Johannesburg, S. Afr.

Weis, D., B. Kieffer, C. Maerschalk, W. Pretorius, and J. Barling (2005), High-precision Pb-Sr-Nd-Hf isotopic characterization of USGS BHVO-1 and BHVO-2 reference materials, *Geochem. Geophys. Geosyst.*, *6*, Q02002, doi:10.1029/2004GC000852.

White, S. H., H. de Boorder, and C. B. Smith (1995), Structural controls of kimberlite and lamproite emplacement, *J. Geochem. Exp.*, *53*, 245–264, doi:10.1016/0375-6742(94)00033-8.

Wilson, L., and J. W. Head (2007), An integrated model of kimberlite ascent and eruption, *Nature*, *447*, 53–57, doi:10.1038/nature05692.

Wu, F. Y., Y. H. Yang, R. H. Mitchell, Q. L. Li, J. H. Yang, and Y. B. Zhang (2010), In situ U-Pb age determination and Nd isotopic analyses of perovskites from kimberlites in southern Africa and Somerset Island, Canada, *Lithos*, *115*, 205–222, doi:10.1016/j.lithos.2009.12.010.

Wu, F. Y., R. H. Mitchell, Q. L. Li, J. Sun, C. Z. Liu, and Y. H. Yang (2013), In situ U-Pb age determination and Sr-Nd isotopic analysis of perovskite from the Premier (Cullinan) kimberlite, South Africa, *Chem. Geol.*, *353*, 83–95, doi:10.1016/j.chemgeo.2012.06.002.

Zonneveld, J. P., B. A. Kjarsgaard, S. E. Harvey, K. Marcia, D. McNeil, and L. M. Heaman (2004), Sedimentologic and stratigraphic constraints on the Star kimberlite, east-central Saskatchewan, *Lithos*, *76*, 115–138, doi:10.1016/j.lithos.2004.03.043.

Zurevinski, S. E., L. M. Heaman, and R. A. Creaser (2011), The origin of Triassic/Jurassic kimberlite magmatism, Canada: Two mantle sources revealed from the Sr-Nd isotopic composition of groundmass perovskite, *Geochem. Geophys. Geosyst.*, *12*, Q09005, doi:10.1029/2011GC003659.